Phage Portal Proteins Suppress Bacterial Stringent Response to Promote Infection

Kristina Kronborg[1#], Luokai Wang[2#], Muriel Schicketanz[1^], Kenn Gerdes[3], Yong Everett Zhang[1*]

[1] Department of Biology, University of Copenhagen, DK-2200 Copenhagen, Denmark

[2] School of Clinical and Basic Medical Sciences, Shandong First Medical University & Shandong Academy of Medical Sciences, Jinan 250117, China.

[3]Independent researcher, Copenhagen, Denmark

[#] K.K. and L.K.W. contributed equally to this work.

^ Current address: Novonesis A/S, Kgs. Lyngby, Denmark

*Correspondence: Yong Everett Zhang zhangy830328@gmail.com

Running title: Phage portal proteins repress the stringent response

Abstract

Bacteriophages must overcome host stress responses to replicate efficiently, yet how they engage with these pathways remains poorly understood. The bacterial stringent response (SR), mediated by the alarmone (p)ppGpp, globally suppresses metabolism and limits biosynthetic capacity, posing a potential barrier to phage infection. Here, we show that bacteriophage T7 directly counteracts the SR through its portal protein, Gp8. Using complementary genetic, biochemical, and infection assays, we demonstrate that Gp8 physically interacts with the (p)ppGpp synthetases RelA and SpoT, selectively inhibiting their synthetase activities and reducing intracellular (p)ppGpp levels during late infection. Disruption of this interaction delays host cell lysis and compromises phage replication, while elevated host (p)ppGpp levels impair infection efficiency. Remarkably, portal proteins from diverse *Escherichia coli* phages share similar structural and functional properties, suggesting a conserved viral strategy to suppress the stringent response. Together, our findings uncover an unexpected regulatory role for phage portal proteins and reveal a conserved mechanism by which phages modulate bacterial stress physiology to optimize replication.

Keywords

Stringent response, ppGpp, pppGpp, alarmone, RelA, SpoT, T7, phage, portal

32 **Introduction**

33 Bacteria continuously encounter environmental stresses that threaten growth and survival. To
34 adapt, they rely on conserved stress response pathways that reprogram cellular physiology in
35 response to nutrient limitation, metabolic imbalance, and environmental insults. Among
36 these, the stringent response (SR) is one of the most ancient and pervasive regulatory systems
37 in bacteria, coordinating a global shift from growth to survival through the alarmone
38 (p)ppGpp[1-4]. Beyond its canonical role in stress adaptation, the SR profoundly influences
39 antibiotic tolerance[5], persistence[6,7], virulence[8], and susceptibility to bacteriophages[9-11].

40 Despite growing recognition that bacterial stress responses shape phage–host interactions[12,13],
41 how phages engage with these pathways remains poorly understood. While the SR has been
42 implicated in limiting phage replication[9-11], the molecular mechanisms underlying this effect -
43 and whether phages actively counteract it - remain largely unexplored.

44 The SR is mediated by the hyperphosphorylated guanine nucleotides ppGpp and pppGpp[4],
45 synthesized primarily by the enzymes RelA and SpoT in *Escherichia coli*[3]. RelA is activated
46 by amino acid starvation[14], whereas SpoT integrates diverse stress signals to maintain
47 (p)ppGpp homeostasis[15-19]. Elevated (p)ppGpp levels remodel transcription by targeting RNA
48 polymerase[20,21], suppressing ribosome biogenesis and nucleotide synthesis while promoting
49 amino acid synthesis and stress resistance[22]. This metabolic state enhances bacterial survival
50 under adverse conditions but also restricts biosynthetic capacity[23].

51 Intriguingly, several observations suggest that the SR may represent a major barrier to
52 productive phage infection. Cells lacking (p)ppGpp display increased susceptibility to T7
53 phage killing[9], whereas stationary-phase cells - characterized by high (p)ppGpp levels - are
54 often less sensitive to infection[24,25]. Conversely, phages appear to have evolved counter-

55 strategies to manipulate the SR. Some phages encode their own (p)ppGpp-modulating
56 toxins[26], while others, like T7, rely on the essential inhibition of the host RNA polymerase -
57 the primary target of (p)ppGpp - to initiate their transcriptional program. Indeed, the well-
58 characterized T7 protein Gp2 is a potent inhibitor of the host RNA polymerase[27].
59 Furthermore, the T7 protein Gp5.7 is critical for infection during stationary phase, a
60 physiological state governed by the (p)ppGpp-dependent general stress regulator RpoS[9].
61 These findings raise the possibility that phages exploit or manipulate the SR to optimize their
62 replication.

63 Here, we investigate the interplay between the stringent response and infection by
64 bacteriophage T7. Using complementary functional screens, biochemical assays, and mutant
65 phages, we identify the T7 portal protein Gp8 as a direct inhibitor of (p)ppGpp synthesis. We
66 show that Gp8 physically interacts with both RelA and SpoT, selectively suppressing their
67 synthetase activities and reducing intracellular (p)ppGpp levels during late infection.
68 Disrupting this interaction compromises phage replication and delays host cell lysis.

69 Remarkably, portal proteins from diverse *E. coli* phages exhibit similar properties, suggesting
70 a conserved viral strategy to disarm a universal bacterial alarm system. Together, our findings
71 reveal an unexpected regulatory role for phage portal proteins and uncover a fundamental
72 mechanism by which phages modulate bacterial stress physiology to promote efficient
73 replication.

74 **Results**

75 **Bacteriophage T7 proteins do not interact directly with (p)ppGpp**

76 Cells lacking (p)ppGpp display increased susceptibility to bacteriophage T7[9], suggesting a
77 functional interplay between the T7 infection cycle and the stringent response (SR). One

78 possibility is that (p)ppGpp directly binds and inhibits phage-encoded proteins. To test this,
79 we cloned the majority of T7 genes (**supplemented document 1**) and screened them for
80 (p)ppGpp binding using DRaCALA. Despite robust assay performance, we detected no
81 specific (p)ppGpp-binding activity among the tested T7 proteins (**supplemented Fig. 1**),
82 indicating that T7 does not encode proteins that directly sense (p)ppGpp. These findings
83 suggest that T7 may instead counteract the SR indirectly, by targeting (p)ppGpp synthesis or
84 signaling.

85 **Many T7 proteins inhibit *E. coli* growth specifically under stringent conditions**

86 If T7 antagonizes the SR, expression of such phage proteins would be expected to
87 compromise bacterial growth under conditions where (p)ppGpp is required (**Fig. 1a**). To test
88 this, we cloned all 53 T7 genes into an inducible expression system (**supplemented file S1**)
89 and assessed their effects on *E. coli* growth in rich and minimal media.

90 Strikingly, 34 of 53 T7 proteins caused severe growth inhibition when expressed in minimal
91 medium, whereas most were non-toxic in rich medium (**Fig. 1b; supplemented Fig. 2**).
92 Toxic proteins were enriched among early and intermediate genes but also included several
93 late structural proteins, suggesting that T7 deploys host-inhibitory activities throughout
94 infection. Notably, many toxic proteins lacked annotated functions, indicating the presence of
95 previously unrecognized phage-host interactions. These results point to a broad T7 strategy
96 targeting host processes that are conditionally essential during nutrient limitation, consistent
97 with interference in stress-response pathways.

98 **Stringent RNA polymerase mutants suppress toxicity of a subset of T7 proteins**

99 To identify T7 proteins that specifically interfere with the SR, we exploited so-called SR-like
100 mutant RNA polymerases ($RNAP^{SR}$) that bypass the requirement for (p)ppGpp to support

101 growth in minimal medium. Toxic T7 genes were expressed in RNAP^{SR} strains (YZ920,
102 *rpoB3449*, ΔAla532[28]; YZ922, *rpoB3443*, L533P[29]) and compared with wild-type cells
103 (**supplemented Fig. 3**).

104 The toxicity of four T7 proteins - Gp1.5, Gp4.2, Gp6.5, and Gp8 - was reproducibly
105 suppressed by the two independent RNAP^{SR} alleles (**supplemented Fig. 4**). Importantly, this
106 suppression persisted in a (p)ppGpp^{0} background lacking RelA and SpoT but harboring
107 the *rpoB3449* allele [28] (**Fig. 1c)**, indicating that RNAP^{SR} -mediated rescue does not require
108 (p)ppGpp itself. These RNAP^{SR} suppression screens narrowed the candidate set to a small
109 group of T7 proteins genetically linked to SR signaling.

110 **Gp8 directly interacts with *E. coli* RelA and SpoT to inhibit (p)ppGpp synthesis**

111 The results above suggested that one or more T7 proteins might directly target key
112 components of the SR, including RelA, SpoT, or RNA polymerase. To test this hypothesis,
113 we employed a bacterial two-hybrid (B2H) assay to systematically assess protein–protein
114 interactions between candidate T7 proteins and SR components.

115 Among the proteins tested, the T7 portal protein Gp8 showed robust interactions with both
116 RelA and SpoT across independent B2H configurations (**Fig. 2a**). These interactions were
117 independently validated by copurification assays using Flag-tagged Gp8 and His–MBP–
118 SUMO–tagged RelA or SpoT, confirming direct physical association *in vitro* (**Fig. 2b**).
119 Instead, no consistent interactions were detected between RelA or SpoT and the other
120 candidate T7 proteins examined.

121 We next asked whether Gp8 binding affected the catalytic activities of RelA and SpoT. To
122 address this, we purified Gp8, RelA, and SpoT variants selectively retaining synthetase or
123 hydrolase activity (YZ1632, YZ1607, YZ1070 and YZ1063, respectively). *In vitro* enzymatic

124 assays revealed that Gp8 potently inhibited the synthetase activities of both RelA and SpoT,
125 with IC_{50} values of 9.71 and 0.53 molar ratios, respectively (**Fig. 2c**). In contrast, Gp8 had no
126 detectable effect on the hydrolase activity of SpoT (**Fig. 2d**), indicating that Gp8 selectively
127 suppresses (p)ppGpp synthesis without perturbing degradation.

128 To determine whether this inhibition occurred *in vivo*, we measured intracellular (p)ppGpp
129 levels following Gp8 expression. Gp8 expression markedly suppressed (p)ppGpp
130 accumulation relative to control conditions (**Fig. 2e, supplemented Fig. 5**), consistent with
131 inhibition of RelA- and SpoT-mediated synthesis *in vivo*.

132 Together, these results demonstrate that the T7 portal protein Gp8 directly inhibits (p)ppGpp
133 synthesis by both RelA and SpoT through physical interaction, providing a molecular
134 mechanism by which T7 suppresses the host SR during infection.

135 **Gp8 residues essential for interaction with RelA and SpoT**

136 The T7 portal protein Gp8 assembles into a dodecameric ring composed of four structured
137 domains-clip, stem, wing, and crown-forming a central channel for phage DNA
138 translocation[30]. Structural analyses indicate that the exterior surface of the ring is
139 predominantly negatively charged, with acidic residues distributed across the wing, stem, and
140 crown domains, interrupted only by a narrow positively charged region near the clip domain
141 (**Fig. 2f**).

142 To define the regions of Gp8 required for interaction with RelA and SpoT, we generated a
143 series of domain truncations and tested their interactions using the bacterial two-hybrid
144 (B2H) assay (**Fig. 3**). Deletion of either the N- or C-terminal regions of Gp8 abolished
145 interactions with both RelA and SpoT (**Fig. 3a**). In contrast, deletion of the clip domain
146 modestly enhanced interaction signals, whereas further deletion extending into the stem

147 domain eliminated interactions. These results indicate that an intact Gp8 ring structure is
148 required for interaction with RelA and SpoT and suggest that the clip domain may negatively
149 modulate accessibility of the interaction interface.

150 Given the strongly electronegative surface of the Gp8 ring, we next tested whether
151 electrostatic interactions contribute to RelA and SpoT binding. We generated 43 charge-
152 reversal mutants targeting clusters of surface-exposed acidic and basic residues and assessed
153 their interactions with RelA and SpoT using the B2H assay (**supplemented Fig. 6**).

154 Approximately half of the mutants exhibited substantial loss of interaction with RelA, and the
155 same mutations similarly impaired SpoT binding (**supplemented Fig. 6a–e**). Several charge-
156 reversal mutations (for example, D220R/E221R, D457K/D460K, E280R/E284R, K4D/R5D,
157 and K288D/K295D) completely abolished interaction, whereas others caused partial defects.
158 These results identify discrete charged regions on the Gp8 surface that are critical for
159 interaction with both RelA and SpoT (**Fig. 3b**), supporting an electrostatically mediated
160 binding mechanism.

161 To identify the corresponding interaction regions on RelA and SpoT, we generated domain
162 truncations of both proteins and tested their ability to interact with wild-type Gp8. Removal
163 of the N-terminal catalytic domains of SpoT abolished its interaction with Gp8, whereas
164 truncation of the C-terminal ACT and CC regulatory domains of RelA disrupted binding
165 (**Fig. 3c, 3d**). These results indicate that Gp8 engages RelA and SpoT through distinct
166 domain interfaces.

167 **Gp8 promotes efficient phage infection by suppressing (p)ppGpp synthesis**

168 To determine whether Gp8-RelA/SpoT interactions contribute to T7 infection, we generated
169 T7 phages carrying Gp8 mutations that disrupt binding to RelA and SpoT. Using

170 the *trxA* method coupled with Red recombineering[31], we successfully isolated two mutant
171 phages - $T7_{D220R/E221R}$ and $T7_{E10K/D11K}$ - exhibiting complete and partial defects, respectively,
172 in RelA/SpoT interaction (**supplemented Fig. 6**). Impaired binding was confirmed by pull-
173 down assays (**Fig. 4a**).

174 In plaque assays on wild-type *E. coli*, $T7_{D220R/E221R}$ formed significantly smaller plaques than
175 $T7_{wt}$ (plaque diameter 2.7 ± 0.7 vs 4.7 ± 0.6 mm, respectively; Student's t-test, $p<0.0001$),
176 whereas $T7_{E10K/D11K}$ displayed an intermediate phenotype (**Fig. 4b,4c**). When infecting Δ*relA*
177 cells, plaque size increased only for the partially defective $T7_{E10K/D11K}$ mutant, whereas
178 infection of a (p)ppGpp^0 strain increased plaque sizes for all phages tested. These results
179 suggest that Gp8-mediated suppression of (p)ppGpp contributes to efficient plaque formation.

180 We expected the $T7_{D220R/E221R}$ mutant to lyse the (p)ppGpp^0 strain as efficiently as $T7_{wt}$ if its
181 sole defect were impaired inhibition of RelA/SpoT; however, this was not observed (**Fig. 4c**).
182 Because plaque assays can underestimate infection efficiency due to restricted virion diffusion
183 in soft agar, we next assessed infection dynamics using a liquid killing assay. Compared with
184 $T7_{wt}$, $T7_{D220R/E221R}$ exhibited a marked delay in host cell lysis of wild-type *E. coli* (**Fig. 4d**; 25
185 min i.e., 25/44 = 57% delay). This delay was substantially reduced in Δ*relA* and (p)ppGpp^0
186 strains (20- and 6.6-min, i.e. 45% and 15% delay, respectively), indicating that impaired
187 infection of wild-type cells is largely attributable to uncontrolled elevated (p)ppGpp levels.
188 These data demonstrate that Gp8–RelA/SpoT interactions are important for efficient T7
189 infection under physiological conditions.

190 Consistent with this interpretation, increasing host (p)ppGpp levels hindered phage infection.
191 $T7_{wt}$ infection of strains producing elevated (p)ppGpp *(*Δ*relA spoT202* and Δ*relA spoT203*;
192 with 4× and 7× higher (p)ppGpp levels than wt *E. coli,* respectively[32]) resulted in delayed and

193 slower lysis kinetics compared with wt cells (**supplemented Fig. 7a**), supporting an inverse
194 relationship between (p)ppGpp abundance and phage infection efficiency.

195 To directly monitor (p)ppGpp dynamics during infection, we labeled (p)ppGpp with ^{32}P and
196 monitored its dynamics during infection (MOI = 0.1) by $T7_{wt}$ and $T7_{D220R/E221R}$. In $T7_{wt}$
197 infections, (p)ppGpp levels declined immediately prior to lysis, whereas this decline was
198 delayed in cells infected with $T7_{D220R/E221R}$ (**supplemented Fig. 7b–d**). Because (p)ppGpp
199 labeling in LB was inefficient, we repeated the experiment in chemically defined MOPS
200 medium supplemented with 0.2% glucose and low phosphate (0.2 mM), which allowed clear
201 resolution of ATP, GTP, ppGpp, and pppGpp by thin layer chromatography (TLC). Under
202 these conditions, $T7_{D220R/E221R}$ again caused delayed killing relative to $T7_{wt}$ (**supplemented**
203 **Fig. 7e**). Although (p)ppGpp became detectable by 10 min post-infection in both strains
204 (**supplemented Fig. 7f,7g**), substantially higher levels accumulated in $T7_{D220R/E221R}$ –infected
205 cells (**Fig. 4e**), reaching ~20% of the total ATP+GTP+(p)ppGpp pool compared with ~5% in
206 $T7_{wt}$ infections. This sustained elevation of (p)ppGpp correlated with delayed first-cycle lysis
207 of host cells and slower population collapse.

208 Together, these results demonstrate that Gp8 suppresses (p)ppGpp accumulation prior to
209 lysis, thereby promoting efficient lytic progression and phage infection.

210 **Gp8-mediated suppression of the stringent response is conserved among coliphages**

211 Gp8 is highly conserved in phages and is essential for capsid assembly and DNA packaging.
212 To assess whether Gp8-mediated suppression of the SR represents a conserved strategy, we
213 analyzed portal proteins from 18 phylogenetically distinct and representative *E. coli* phages
214 out of the BASEL collection[33]. Structural predictions using AlphaFold3 indicated that most

portal proteins form negatively charged ring-like assemblies similar to T7 Gp8 (**supplemented document 2**).

Consistent with a conserved role for the SR in phage defense, many (11/18) of these phages infected (p)ppGpp^0 cells more efficiently than wt cells, producing larger or clearer plaques or increased plague forming units (PFU) (**supplemented document 2**). To test whether this involved RelA/SpoT, we examined portal proteins from phages P1 and N4. Both were toxic when expressed in *E. coli*, and this toxicity was partially suppressed by RNAP^{SR} alleles (**supplemented Fig. 8**). Both proteins interacted with RelA and SpoT in B2H assays (**Fig. 5a**).

Collectively, these findings indicate that phage portal proteins from diverse lineages interact with RelA and SpoT to modulate the host SR, revealing a conserved viral strategy to overcome bacterial stress defenses.

Discussion

A conserved role for phage portal proteins in repression of the stringent response

In this study, we identify a conserved mechanism by which bacteriophages directly repress the bacterial stringent response (SR) through their portal proteins, essential and ubiquitous components of the viral capsid. We show that the T7 portal protein Gp8 physically interacts with the (p)ppGpp synthetases RelA and SpoT, selectively inhibiting (p)ppGpp synthesis. This conclusion is supported by complementary genetic, biochemical, and infection-based evidence, including direct protein–protein interactions, inhibition of synthetase activity *in vitro*, suppression of (p)ppGpp accumulation *in vivo*, and impaired phage infection when these interactions are disrupted. Importantly, portal proteins from diverse coliphages share

238 similar structural and functional properties, indicating that modulation of the SR by portal
239 proteins represents a broadly conserved viral strategy.

240 These findings expand the current view of phage–host interactions by positioning the SR as a
241 dynamic regulatory axis that phages actively manipulate, rather than merely endure. While
242 the SR is widely recognized as a bacterial defense mechanism that limits phage replication,
243 our results demonstrate that successful phages can both tolerate and exploit this response in a
244 temporally controlled manner.

245 A biphasic model for stringent response modulation during T7 infection

246 Based on our data, we propose a biphasic model for the role of (p)ppGpp during T7 infection
247 (**Fig. 5b**). Early in infection, phage entry and host takeover inevitably trigger stress responses
248 that activate (p)ppGpp synthesis. At this stage, suppression of host metabolism, particularly
249 inhibition of host RNA polymerase, is advantageous to the phage, as it limits competing
250 cellular processes and facilitates the transition to phage-directed transcription[34]. Notably,
251 (p)ppGpp preferentially inhibits *E. coli* RNA polymerase while having little effect on T7
252 RNA polymerase[35,36], allowing phage transcription to proceed efficiently. This effect is
253 reinforced by multiple T7-encoded inhibitors of host RNA polymerase (Gp2[37], Gp5.7[9],
254 Gp0.7[38]), underscoring the importance of early host transcriptional shutdown for productive
255 infection[34].

256 As infection progresses, however, the physiological requirements of the phage shift. Late
257 stages of infection involve massive synthesis of structural proteins and energy-intensive
258 genome packaging by the terminase–portal complex, processes that place high demands on
259 cellular amino acids and nucleotide pools[39,40]. Uncontrolled (p)ppGpp accumulation becomes
260 detrimental at this stage, as it depletes ATP and GTP and further suppresses their

261 biosynthesis[41-44]. Our data indicate that Gp8-mediated inhibition of RelA and SpoT alleviates
262 this constraint by suppressing (p)ppGpp levels prior to lysis, thereby restoring nucleotide
263 availability and enabling efficient virion assembly and release.

264 In this framework, the portal protein functions as a molecular gatekeeper that coordinates the
265 transition from early host metabolic repression to late-stage resource mobilization, ensuring
266 optimal timing of lysis and maximal phage yield.

267 Multifunctional phage proteins and conditionally essential host processes

268 The identification of a regulatory role for the portal protein highlights a broader principle in
269 phage biology: the evolution of multifunctional proteins that target host processes essential
270 under specific physiological conditions. Such functional layering is not unique to Gp8. For
271 example, T7 lysozyme (Gp3.5) not only mediates host cell lysis but also regulates T7 RNA
272 polymerase to coordinate transcription and replication[45,46]. These dual-purpose proteins
273 enable phages to maximize functional output from compact genomes.

274 Consistent with this idea, our functional screens revealed numerous T7 proteins that are toxic
275 specifically under nutrient-limited conditions but not in rich media. This conditional toxicity
276 suggests that phages encode factors targeting host pathways that become essential during
277 stress, a context frequently encountered in natural and clinical environments but rarely
278 captured in standard laboratory assays. As bacteria in nature often reside in nutrient-poor or
279 otherwise stressful niches, phage strategies that exploit stress-adapted host physiology are
280 likely widespread and ecologically relevant.

281 Deciphering the targets and mechanisms of these conditionally toxic phage proteins will be
282 critical for a comprehensive understanding of phage infection dynamics in realistic
283 environments. Our findings establish a conceptual framework for exploring how phages

engage bacterial stress responses and provide a foundation for uncovering additional, previously hidden layers of phage–host coevolution.

286 **Figures and Legends**

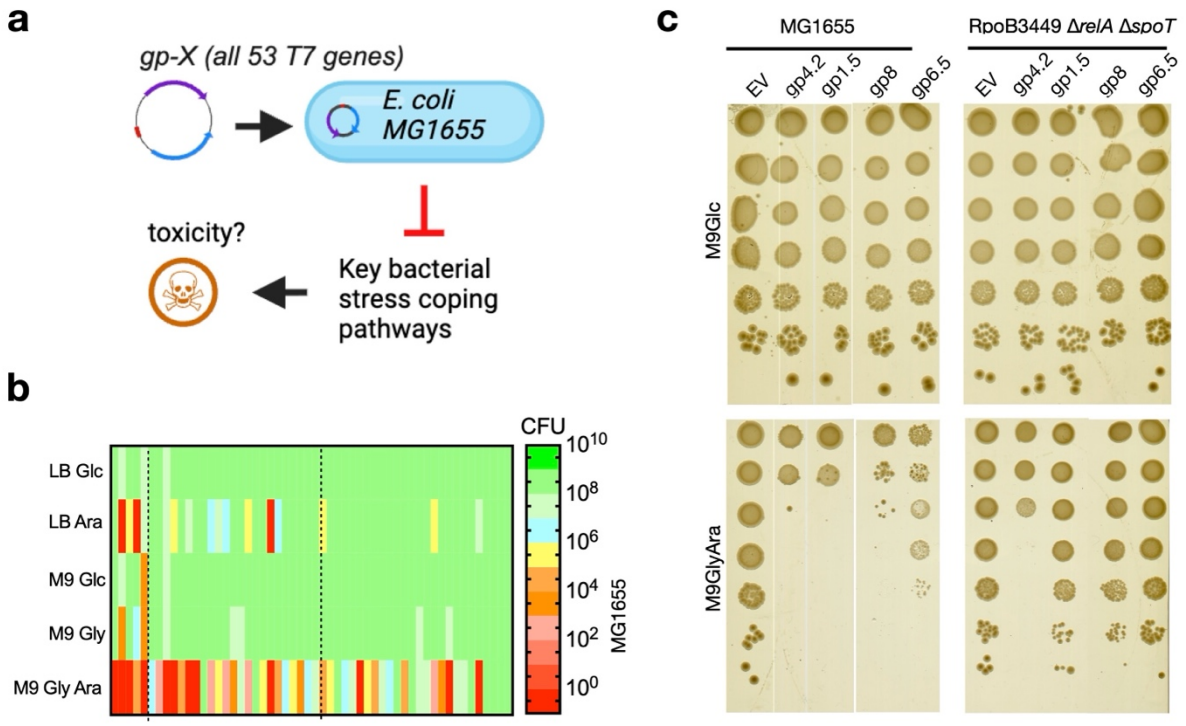

287

288 **Figure 1. Systematic screening of T7 proteins interfering the stringent response in *E.***
289 ***coli*.** (**a**) Scheme of screening for T7 toxic proteins to *E. coli* on M9 minimal medium. See
290 Material and Methods for details. (**b**) Heatmaps summarizing the CFUs/ml/OD_{600nm} of *E. coli*
291 cells expressing each individual T7 proteins on five different media. Glucose and arabinose
292 were used to suppress and induce the expression of T7 genes on pBAD33 plasmid,
293 respectively. LB Glc and LB Ara are LB media supplemented with 0.2% glucose and 0.2%
294 arabinose, respectively. M9 Glc, M9 Gly and M9 Gly Ara are M9 media supplemented with
295 0.4% glucose, 0.4% glycerol and 0.4% glycerol+0.2% arabinose, respectively. See
296 **supplemented Figure S2** for original plate growth. (**c**) Ten-fold serial dilutions (top to
297 bottom) of WT MG1655 or an isogenic *ΔrelA ΔspoT* strain carrying the SR-like mutation
298 *rpoB3449* were spotted on M9Glc or M9GlyAra plates. Cells expressed the indicated T7
299 genes (gp4.2, gp1.5, gp8, gp6.5) or an empty vector (EV). Plates were photographed after 72
300 h of growth at 37 °C.

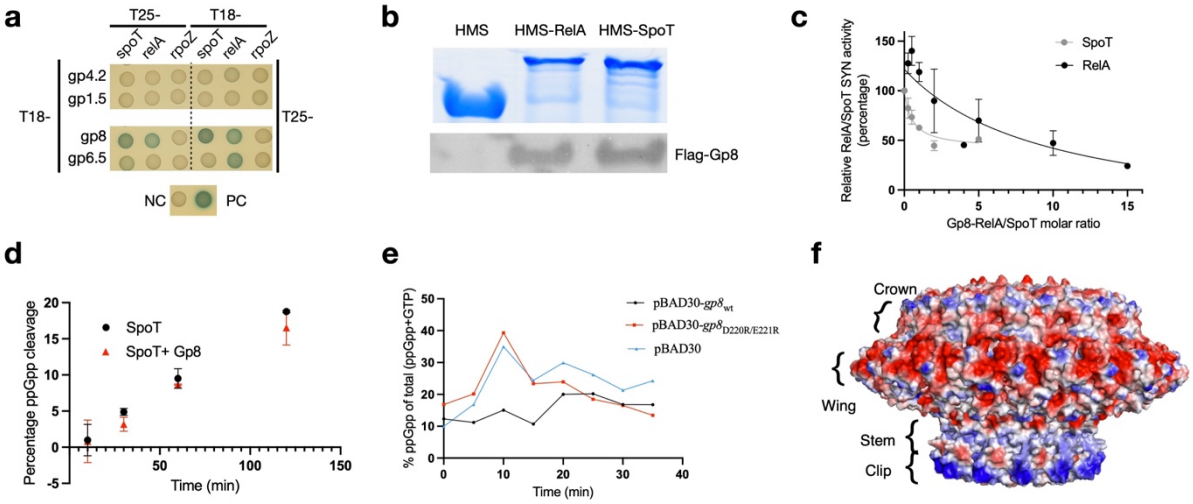

Figure 2. Gp8 directly inhibits the synthetic activities of RelA and SpoT. (**a**) Bacterial two-hybrid assays assessing interactions between Gp8, Gp4.2, Gp1.5, and Gp6.5 with RelA, SpoT, and RpoZ (the ω-subunit of RNAP). NC and PC denote negative and positive controls, respectively. (**b**) Pull down assays using the HMS (Histidine6-MBP-SUMO) tag, HMS-RelA, or HMS-SpoT on Flag tagged Gp8. Top, SDS-PAGE of the bait proteins; bottom, Western blot of Flag-Gp8 probed with anti-Flag antibody. (**c**) Synthetase activity assays of RelA and SpoT with increasing molar ratios of Gp8. Activities were normalized to the no-Gp8 condition. Data represent the mean ± SD of three replicates. (**d**) SpoT hydrolytic activity in the absence and presence of Gp8. Data represent three biological replicates. (**e**) Quantification of the percentage of ppGpp relative to total ppGpp+GTP in cells expressing wild-type or mutant Gp8, or an empty vector pBAD30. The corresponding thin layer chromatography plate is shown in **supplemented Figure S5**. (**f**) Electrostatic surface charge of the T7 dodecameric portal complex (PDB: 7EY6).

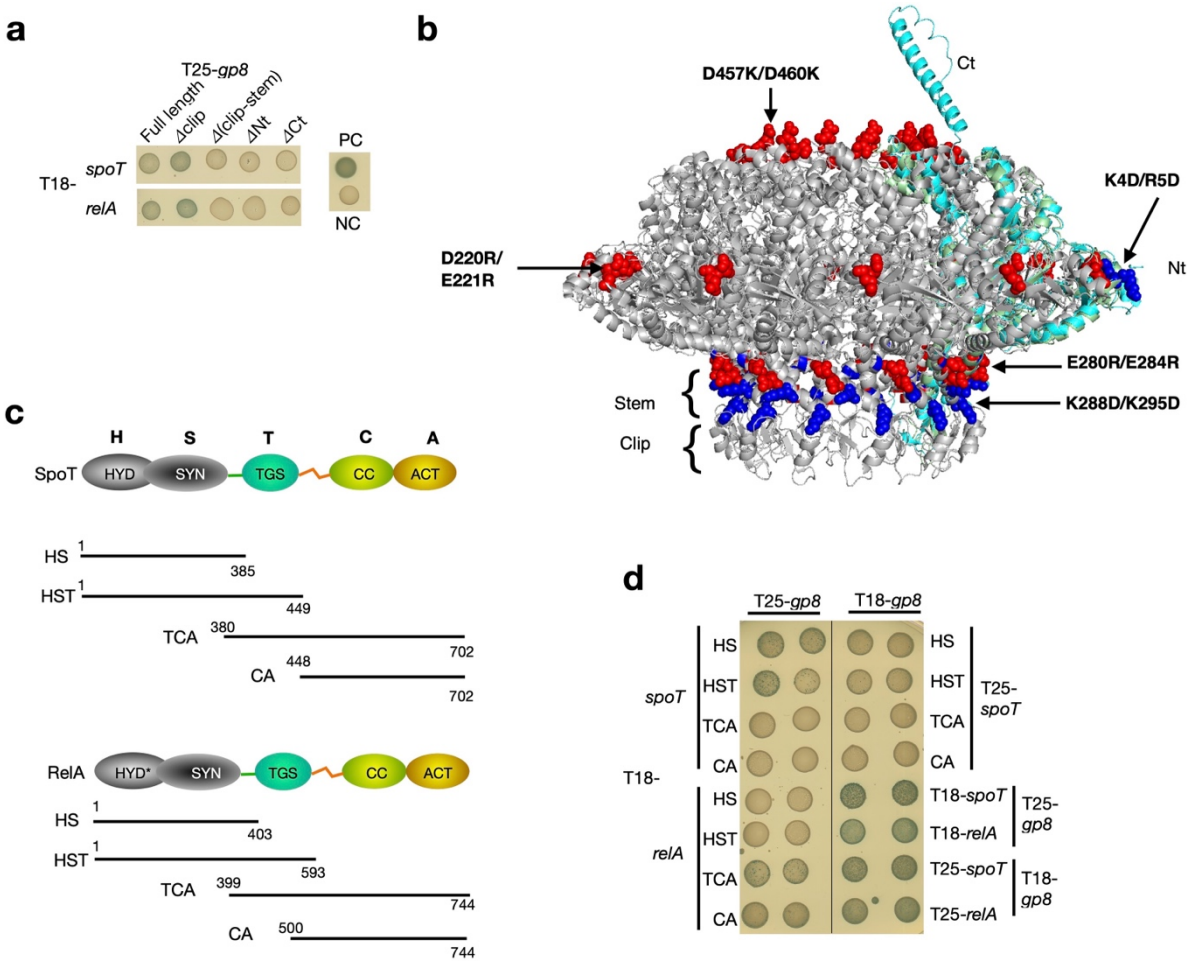

316

317 **Figure 3. Genetic analysis of the interactions between RelA and SpoT, and Gp8.**

318 (**a**) Bacterial two-hybrid assays examining interactions between Gp8 truncations and full-

319 length RelA or SpoT. Δclip, deletion of residues 299–330; Δ(clip-stem), deletion of residues

320 269–355; ΔNt, deletion of residues 6–42; ΔCt, deletion of residues 484–543. NC and PC

321 denote negative and positive controls, respectively. (**b**) Gp8 portal ring (grey, ribbon model,

322 PDB 7EY6) with the mutagenized residues highlighted in red (negatively charged) or blue

323 (positively charged). The AlphaFold model of full-length Gp8 (cyan) is shown overlaid with

324 a single Gp8 monomer (green) to indicate the N- and C-terminal regions, including the

325 mutated K4 and R5 residues. Mutants that lose interaction with RelA/SpoT are shown as

326 spheres and labeled. (**c**) Schematic overview of RelA and SpoT domain architectures and the

327 truncation constructs tested in panel (**d**). Start and end residue numbers are indicated. (**d**)

328 Bacterial two-hybrid assays assessing interactions between Gp8 and the RelA/SpoT

329 truncations shown in (**c**). Two biological replicates are shown side by side.

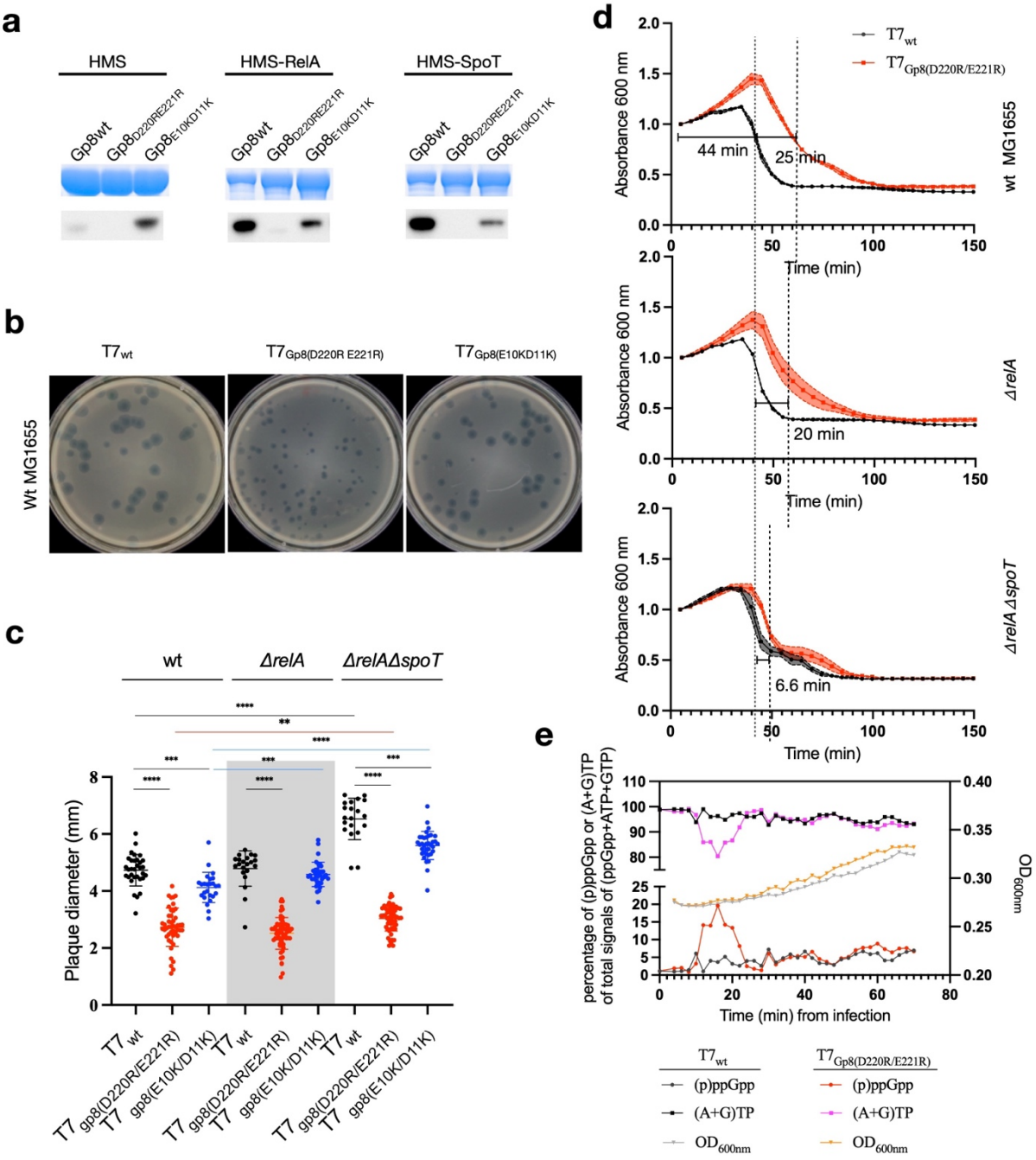

330

331 **Figure 4. Portal interactions with RelA and SpoT enhance infection efficiency.** (**a**) Pull-

332 down assays using HMS-tag, HMS-RelA, or HMS-SpoT as bait with Flag-tagged wild-type

333 (WT) or mutant Gp8 proteins. Top: SDS–PAGE of the bait proteins; bottom: Western blot of

334 Flag-Gp8 probed with anti-Flag antibody. (**b**) Representative plaque morphologies of WT or

335 mutant T7 phages infecting WT *E. coli* MG1655 cells 18 h post-infection. (**c**) Scatter plot of
336 plaque sizes (corresponding to panel **b**) for WT and mutant T7 phages infecting WT, *ΔrelA*,
337 or (p)ppGpp⁰ (*ΔrelA ΔspoT*) strains. **, ***, **** indicate Student's *t*-test $p < 0.01$, 0.001,
338 and 0.0001, respectively. (**d**) Liquid infection assays of WT or mutant T7 phages infecting
339 WT, *ΔrelA*, or (p)ppGpp⁰ (*ΔrelA ΔspoT*) strains. Dashed lines mark the time points at which
340 half of the total decrease in OD_{600nm} before and after lysis occurred; the corresponding
341 durations and difference are indicated. (**e**) Quantification of ATP, GTP, and (p)ppGpp levels
342 in radiolabeled *E. coli* MG1655 cells following infection with WT or mutant T7 phage.
343 OD_{600nm} values of both host cultures are plotted on the secondary (right) Y-axis. Assays were
344 performed in MOPS medium supplemented with 0.2 mM K_2HPO_4 and 0.2% (g/ml) glucose.
345 Raw thin layer chromatography plates are shown in **Figure S7**. The first cycle of cell lysis
346 occurred ca. 30 minutes post infection.
347

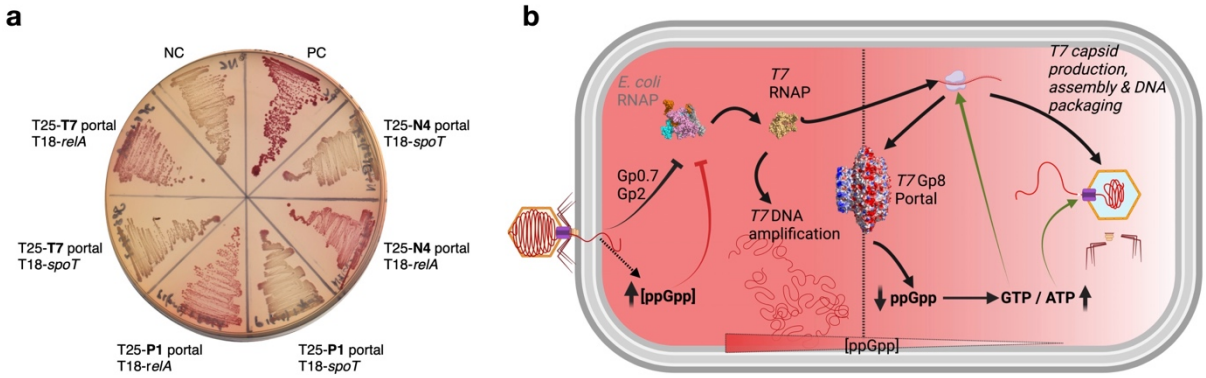

348

349 **Figure 5. Model of how portal protein controls stringent response for efficient phage**
350 **infection.** (**a**) Bacterial two-hybrid assays testing the interactions between RelA/SpoT and
351 portal proteins of phages P1, N4 and, as controls, T7. NC, PC: negative and positive controls,
352 respectively. (**b**) Biphasic model of host resource control during T7 infection. (Left) Early
353 Infection: Phage invasion stress triggers ppGpp production. Host *E. coli* RNAP is inhibited by
354 (p)ppGpp, Gp2, and Gp0.7, enabling a switch to T7 RNAP for middle/late gene transcription.
355 (Right) Late Infection: The structural protein Gp8 (portal vertex) plays a second, non-structural

356 role by suppressing (p)ppGpp. This preserves and derepresses GTP/ATP synthesis, fueling the
357 massive GTP-dependent translation and ATP-dependent DNA packaging required for virion
358 assembly. *E. coli* RNAP, from PDB 4JK1; T7 RNAP, from PDB 1CEZ; T7 Gp8, from PDB
359 7EY6.

360 **Supplementary figures**

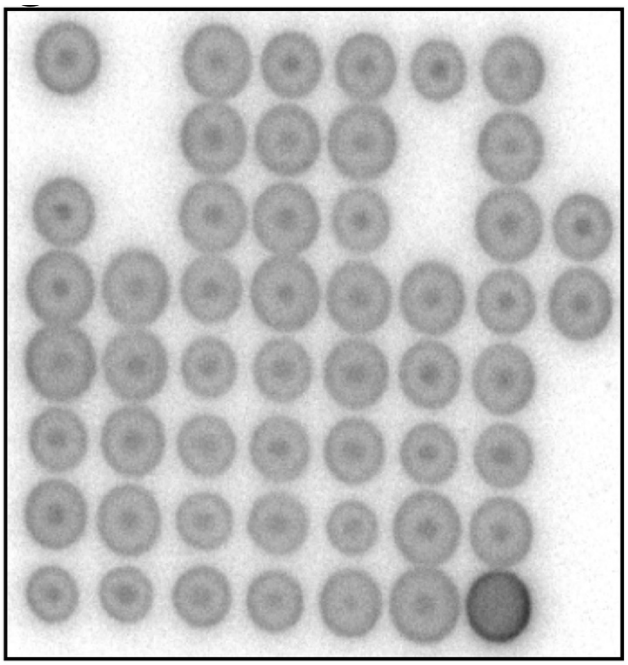

gp0.3		gp1.2	gp1.6	gp2.5	gp3.8	gp4.2	
gp0.4	gp0.7	gp1.3	gp1.7	gp2.8		gp4.3	
gp0.5		gp1.4	gp1.8	gp3		gp4.5	gp5.5
gp0.6A	gp1.1	gp1.5	gp2	gp3.5	gp4.1	gp4.7	gp5.7
gp5.9	gp6.7	gp8	gp11	gp15	gp18	gp19.2	
gp6	gp7	gp9	gp12	gp16	gp18.5	gp19.3	
gp6.3	gp7.3	gp10A	gp13	gp17	gp18.7	gp19.5	
gp6.5	gp7.7	gp10B	gp14	gp17.5	gp19		

361

362 **Figure S1. DRaCALA screen of T7 proteins binding to (p)ppGpp.** (Top) Representative

363 screening plates. The spot at the bottom right corner shows the buffer binding control. (Bottom)

364 The identity of each protein spot is indicated in the table. See Materials and Methods for details.

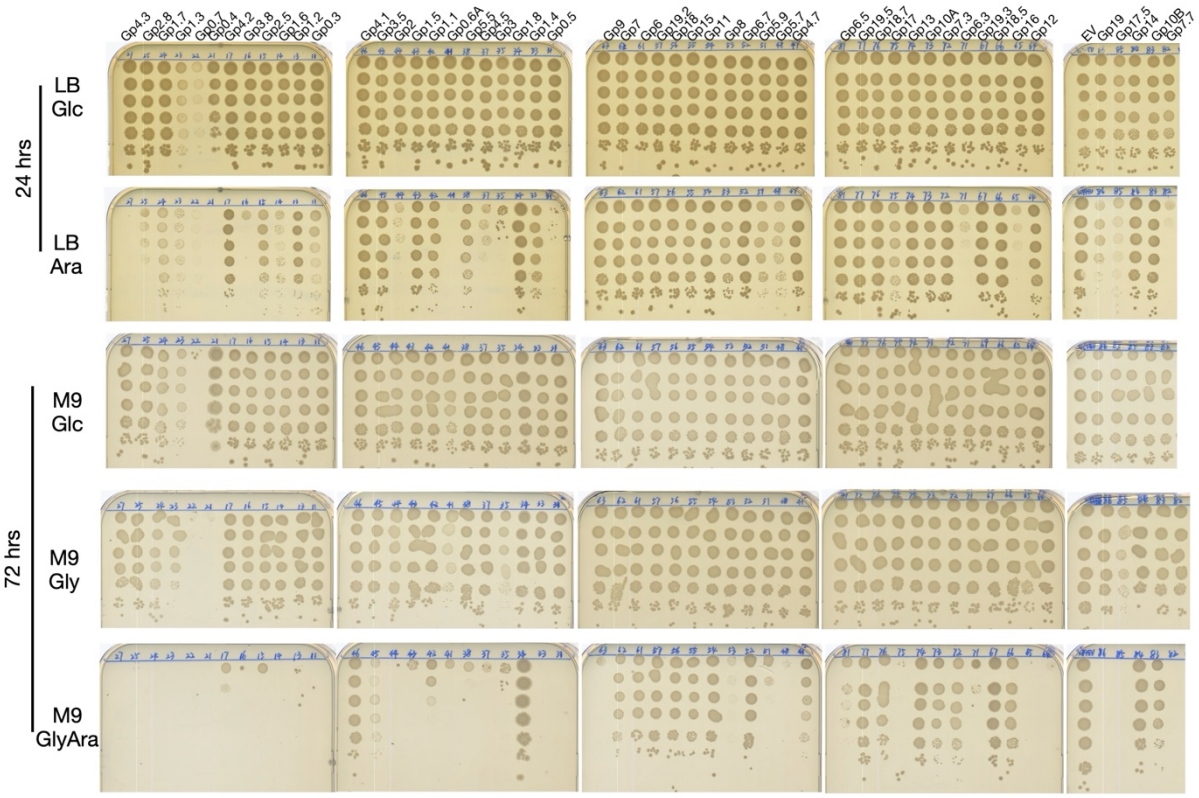

Figure S2. Toxicity test of T7 proteins in *E. coli* MG1655 across five different media. Cells were spotted as serial 10-fold dilutions of normalized culture densities onto the indicated media and incubated at 37 °C. Images for LB Glc and LB Ara plates were taken after 24 h, whereas images for M9-based media were taken after 72 h. The T7 proteins tested are indicated above each plate. EV, empty vector control.

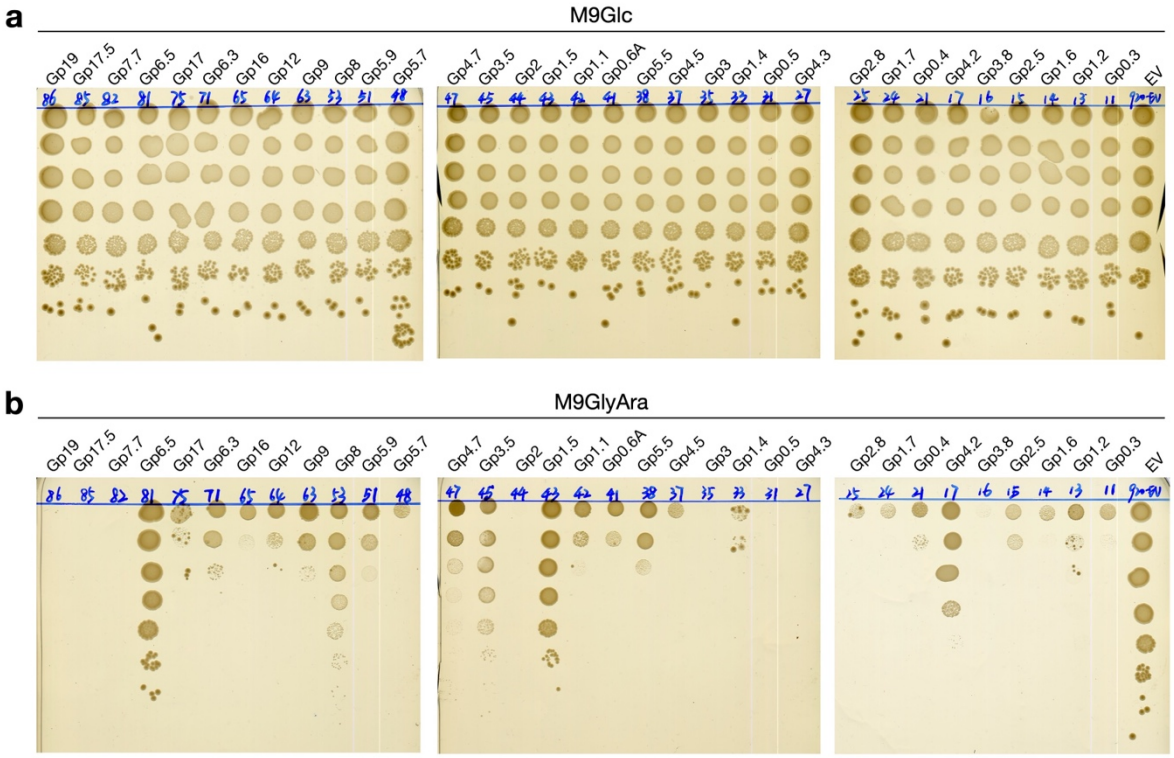

Figure S3. Screening of toxic T7 proteins suppressed by a stringent-like RNAP^{SR} strain. The YZ920 strain carrying the stringent-like *rpoB3449* mutation was transformed with pBAD33 constructs expressing T7 proteins that exhibited toxicity in the wild-type MG1655 strain (see **Figure S2**). Cells were tested on M9Glc (**a**) or M9GlyAra (**b**) media and incubated for 72 h.

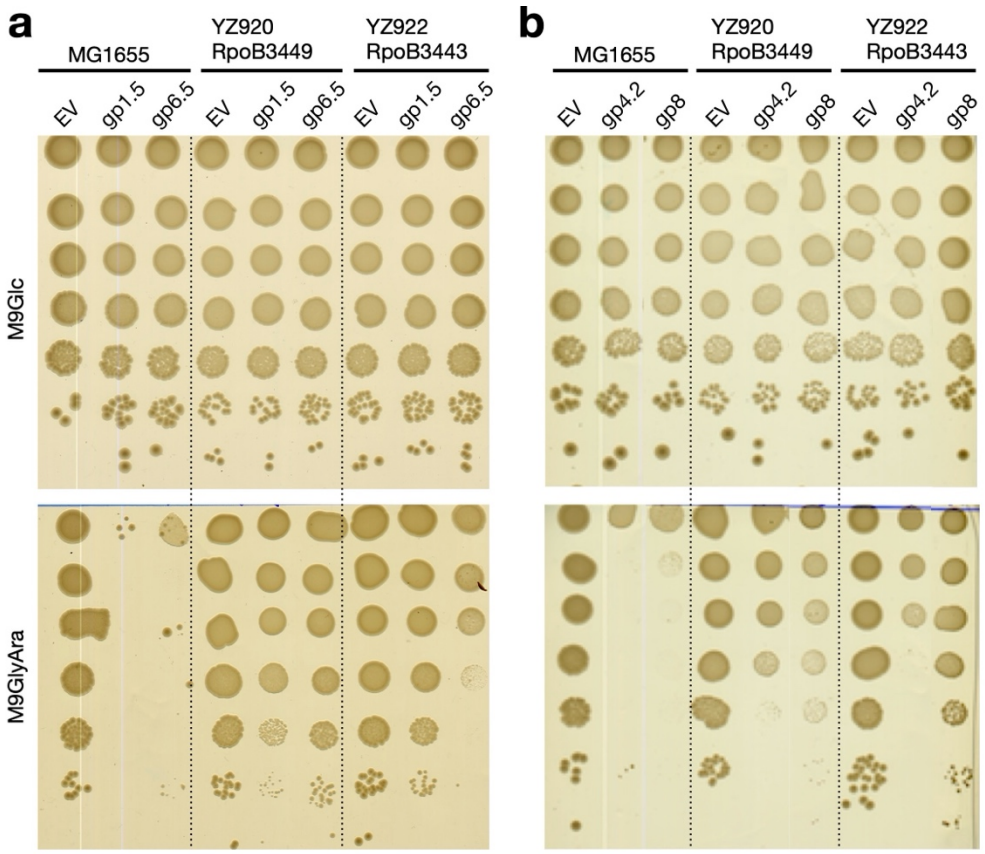

378

379 **Figure S4. Suppression of T7 proteins toxicities by stringent-like RNAP^{SR} strains.** Ten-

380 fold serial dilutions (top to bottom) of WT MG1655 or YZ920 and YZ922 strains carrying the

381 stringent-like *rpoB3449 and rpoB3443* mutations were spotted on M9Glc or M9GlyAra plates.

382 Cells expressed the indicated T7 genes (*gp4.2*, *gp1.5*, *gp8*, *gp6.5*) or an empty vector (EV).

383 Plates were photographed after 72 h of growth at 37 °C.

384

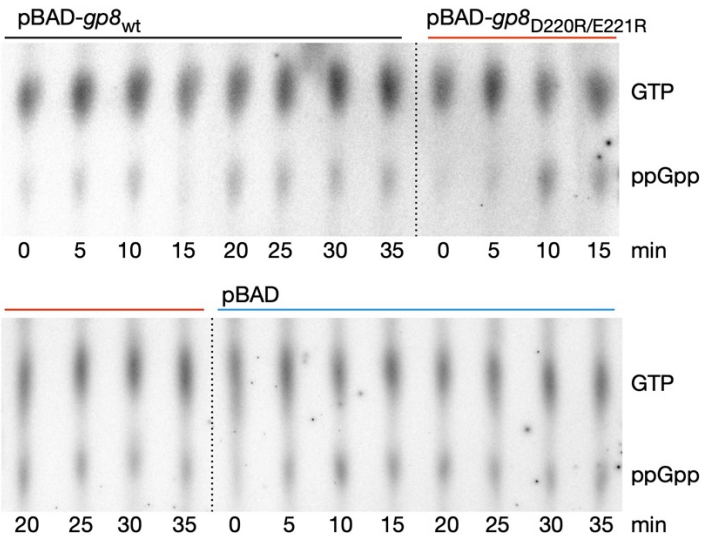

Figure S5. Thin layer chromatography (TLC) analysis of ^{32}P-labeled (p)ppGpp during expression of wild-type and mutant *gp8*$_{D220R/E221R}$ from the pBAD30 vector. Expression of gp8 was induced with 0.2% arabinose, and 25 µL of each sample was assessed by TLC plate (see Materials and Methods for details). GTP and ppGpp spots, as well as the time points (in minutes) after arabinose induction, are indicated.

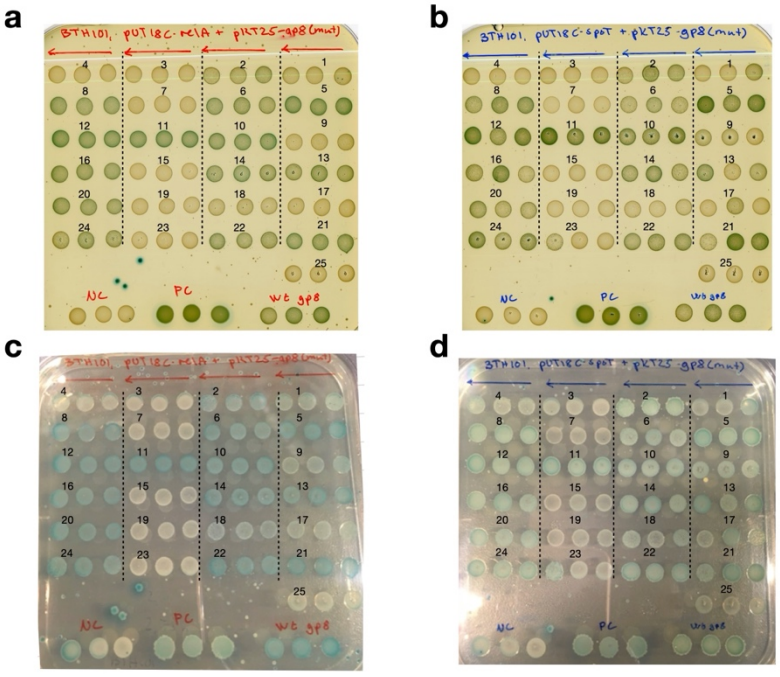

e

1	*D46K/D48K/D53K*
2	D99K/D101K
3	D220R/E221R/D222R/E225R
4	**D220R/E221R**
5	D222R/E225R
6	D241K
7	**D457K/D460K**
8	D502R
9	*E10K/D11K*
10	E149K/E151K
11	E192R/D193K
12	E199R/E204R
13	E236R
14	E247R
15	**E280R/E284R**
16	E416K/E423K
17	*E485K/E486K*
18	*E521R/D528R*
19	**K4D/R5D**
20	K94D
21	K105E
22	K196E
23	**K288D/K295D**
24	K419D
25	*R277D*

393 **Figure S6.** Bacterial two-hybrid assays testing the interactions between Gp8 mutants and
394 RelA (**a,c**), and SpoT (**b,d**). Three replicate spots are shown for each mutant, with the
395 numbers indicating the mutants that are specified in panel (**e**), wherein mutants shown in bold
396 are the more defective ones. Mutants shown in italics are the ones partially defective in
397 RelA/SpoT interaction.
398

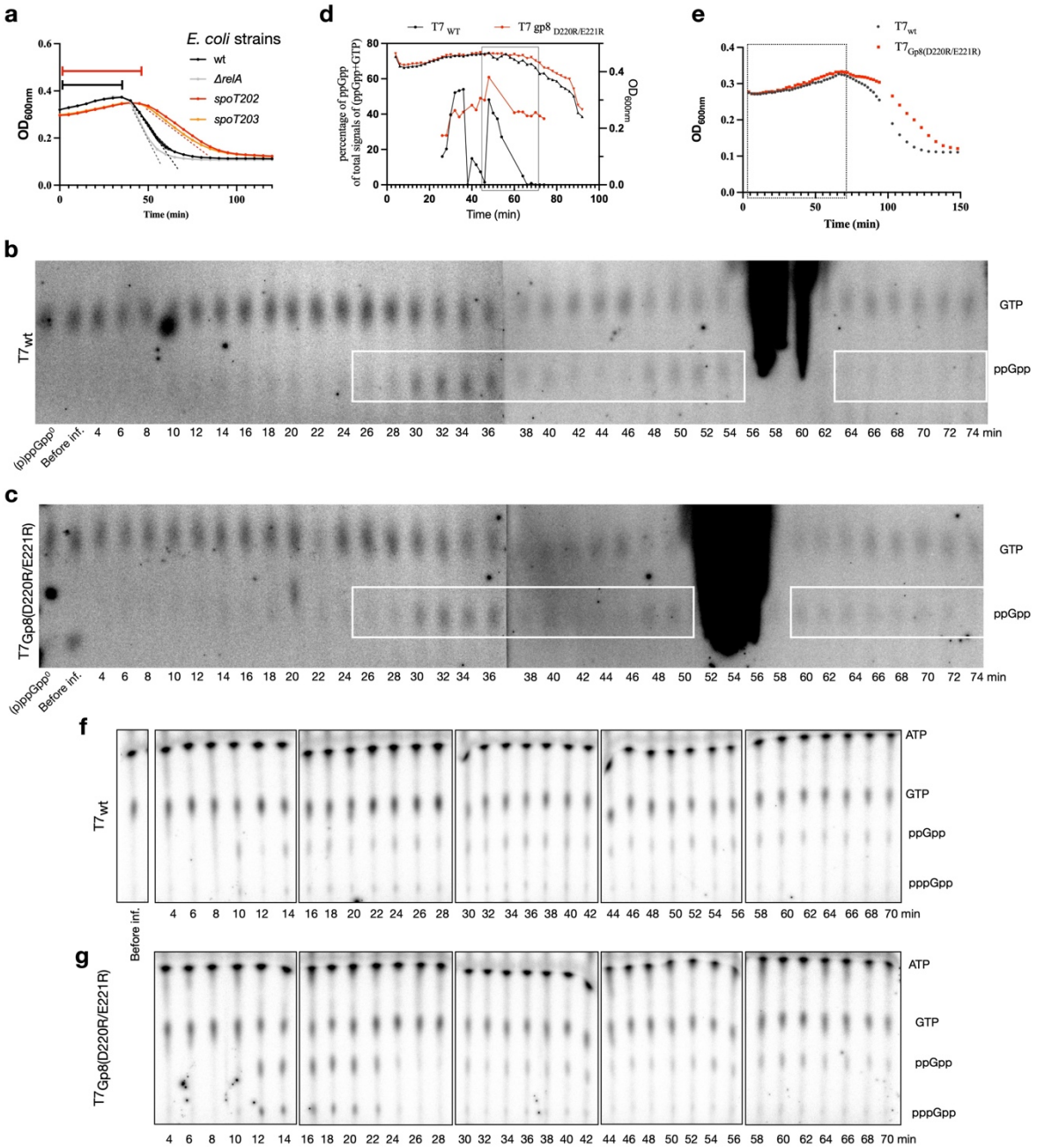

Figure S7. Radiolabeling assays show (p)ppGpp levels during infection with T7 encoding mutant Gp8. (**a**) Liquid infection assays of wt T7 infecting different *E. coli* strains. *spoT202* and *spoT203* have 4× and 7× higher basal level of (p)ppGpp, respectively. The lag phase lengths and the cell lysis slopes are indicated. (**b,c**) ^{32}P labelling of T7 encoding wt (**b**) and mutant (**c**) *gp8* during infection of *E. coli* MG1655 in LB medium. White boxes indicate ppGpp spots. The big black areas are contamination. (**d**) Quantification of ppGpp and OD_{600nm} (plotted to the right Y axis) form the labelling shown in (**b**) and (**c**). (**e**) Lysis curve of *E. coli* MG1655

407 during infection with wt and mutant *gp8*. Box in (**e**) indicates the time points quantified and
408 presented in **Figure 4E**. (**f,g**) ^{32}P labelling of T7 encoding wt (**f**) and mutant (**g**) *gp8* during
409 infection of *E. coli* MG1655 in MOP S medium. Note that quantification methods differ
410 between assays performed in LB (**b-d**) and in MOPS (**e-g**). In LB, only GTP and ppGpp spots
411 are visible, and quantification is expressed as percentage of ppGpp relative to total signal
412 (GTP+ppGpp). In MOPS medium, ATP, GTP, ppGpp and pppGpp are detectable, and
413 quantification is expressed as the percentage of (p)ppGpp relative to the sum of the total signal
414 (ATP+GTP+(p)ppGpp). These differences account for the differing (p)ppGpp percentages
415 displayed here in (**d**) and in **Figure 4e**.
416

417

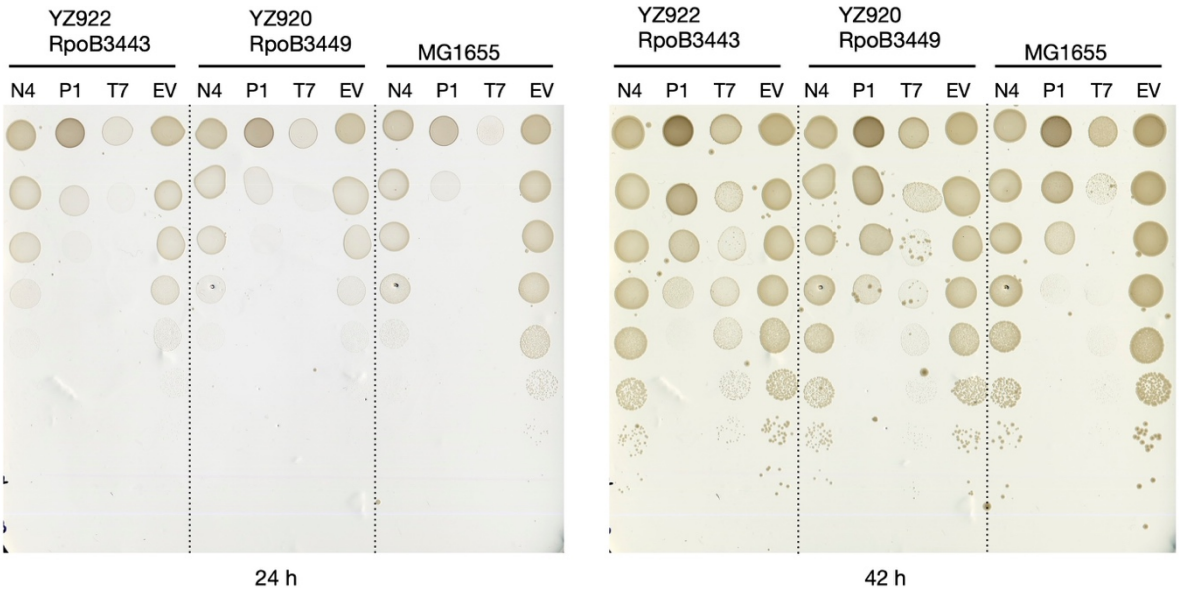

418

419 **Figure S8. Toxicity assay of portal proteins from phages N4 and P1.**
420 Portal proteins from phages N4 and P1 were cloned into the pBAD33 plasmid and expressed
421 in WT MG1655 and in the stringent mutants YZ920 and YZ922, which carry the *rpoB3449*
422 and *rpoB3443* alleles, respectively. Toxicity was assessed on M9 medium supplemented with
423 0.4% glycerol and 0.2% arabinose. Images were taken after 24 and 42 h of incubation at 37°C.
424 N4, P1, and T7 indicate portal proteins from the respective phages; EV denotes the empty-
425 vector control.

426 **Materials and Methods**

427 **Cloning all T7 genes into the pET28b and pBAD33 vectors**

428 Genomic DNA of *E. coli* T7 bacteriophage was used as the template for amplification of
429 individual T7 genes with Q5 High-Fidelity DNA polymerase (New England Biolabs). PCR
430 amplicons were gel-purified, quantified spectrophotometrically, and digested with *EcoRI* and
431 *NcoI* at 37°C for 3 h followed by enzyme inactivation at 80°C for 20 min. The digested
432 fragments were ligated into the similarly treated pET28b vector using T4 DNA ligase at room
433 temperature for 30 min. Ligation mixtures were transformed into chemically competent *E. coli*
434 DH5α cells and plated on LB agar supplemented with kanamycin (25 μg mL^{-1}). Individual
435 transformants were screened by colony PCR, and clones displaying expected insert sizes were
436 cultured in LB medium for plasmid purification. All constructs were verified by Sanger
437 sequencing, yielding a pET28b–T7 gene library encompassing 51 of 59 targeted genes; 8
438 highly toxic genes could not be cloned or yielded unstable plasmids.

439

440 To place the T7 genes under the arabinose-inducible promoter, verified pET–T7 plasmids were
441 digested with *XbaI*, *HindIII* and *EcoRV*, and ligated into pBAD33 linearized with *XbaI* and
442 *HindIII*. This procedure transferred the pET Shine-Dalgarno sequence and corresponding T7
443 gene inserts into pBAD33 under the control of the pBAD promoter. Using the iVEC cloning
444 strategy[47], we successfully obtained pBAD33-*gp0.4* and pBAD33-*gp0.7* plasmids, the pET
445 versions of which were impossible. The resulting library, designated pBAD–T7, comprised 53
446 of 59 T7 genes. For expression of T7 proteins in strain YZ921, the T7 genes were subcloned
447 from the pBAD33 (cat) vector into the pBAD30 (bla) vector using the *XbaI* and *HindIII*
448 restriction sites, as YZ921 carries a chloramphenicol resistance gene (cat).

449

450 **DRaCALA assay**

451 To identify T7 proteins that interact with (p)ppGpp, we carried out a DRaCALA assay
452 following previously described methods[48,49]. In brief, BL21(DE3) strains harboring individual
453 pET28-T7 constructs (**supplemented document 1**) were cultured overnight at 30°C in 1 mL
454 LB supplemented with 25 μg/mL kanamycin in 96-deep-well plates (Greiner). Subsequent
455 steps, including protein induction, cell lysis, and the DRaCALA procedure, were performed as
456 previously described[48,49].
457
458 **Toxicity assay of pBAD33-T7 genes on five media**
459 Each of the 53 verified pBAD–T7 plasmids was individually transformed into chemically
460 competent *E. coli* MG1655 cells. Transformants were streaked as single colonies on LB agar
461 plates supplemented with chloramphenicol (25 μg mL^{-1}) and a single colony from each
462 transformant was inoculated into 1 mL LB broth and cultured overnight at 37°C with shaking
463 (200 rpm). From each culture, 300 μL was diluted in 800 μL fresh LB to measure optical
464 density at 600 nm (OD_{600nm}), while another 300 μL aliquot was pelleted by centrifugation at
465 13,000 rpm for 3 min, washed twice with 1 mL PBS, and resuspended to an OD_{600nm} = 1. Serial
466 tenfold dilutions (10^8–10^1 CFU mL^{-1}) were prepared in 96-well plates by mixing 20 μL of
467 bacterial suspension with 180 μL PBS per well. From each dilution, 5 μL was spotted onto five
468 pre-dried chloramphenicol-containing agar media: LB + 0.4% glucose, LB + 0.2% L-arabinose,
469 M9 + 0.4% glucose, M9 + 0.4% glycerol, and M9 + 0.4% glycerol + 0.2% L-arabinose. Plates
470 were incubated at 37°C and photographed every 24 h to monitor colony growth and induction-
471 dependent phenotypic changes.
472
473 **Construction of bacterial two-hybrid vectors**
474 *Cloning relA, spoT and their truncates*

475 *spoT* and *relA* were cloned into the bacterial two-hybrid vectors pUT18C and pKT25. The
476 full-length genes were amplified from *E. coli* MG1655 chromosomal DNA using primer pairs
477 pYZ479/pYZ480 (*spoT*) and pYZ481/pYZ482 (*relA*). PCR products and recipient plasmids
478 were digested with *XbaI* and *XmaI*, ligated, and transformed into *E. coli*. Truncated *spoT*
479 variants corresponding to the HS, HST, TCA, and CA regions were generated by PCR using
480 primer pairs pYZ473/pYZ474, pYZ473/pYZ475, pYZ477/pYZ476, and pYZ478/pYZ476,
481 respectively. The resulting fragments were digested with *XbaI*/*XmaI* and cloned into pUT18C
482 or pKT25. Truncated *relA* variants (HS, HST, TCA, and CA) were amplified using primer
483 pairs pYZ917/pYZ919, pYZ917/pYZ918, pYZ920/pYZ921, and pYZ920/pYZ922,
484 respectively, digested with *XbaI*/*XmaI*, and cloned into pUT18C.

485 *Cloning of the portal protein from phages P1 and N4 into pKT25*
486 Portal protein from phages P1 and N4 were amplified using primer pairs pYZ1285/pYZ1286
487 and pYZ1287/pYZ1288 for phage P1 and N4, respectively. The pKT25 was digested with *KpnI*
488 and *EcoRI*, assembled with both PCR products by the iVEC cloning method[47].
489 *pUT18-rpoZ and pKNT25-rpoZ*
490 To generate pUT18-*rpoZ*, the full-length *rpoZ* gene was PCR-amplified from *E. coli* MG1655
491 genomic DNA using primers pYZ867 and pYZ868. The amplified fragment and pUT18 vector
492 were digested with *HindIII* and *XbaI*, ligated, and transformed into *E. coli* DH5α. For
493 construction of pKNT25-*rpoZ*, the pKNT25 vector was first modified by site-directed
494 mutagenesis using primers pYZ871 and pYZ872 following the QuickChange protocol to
495 introduce an *NcoI* restriction site, generating pKNT25-*NcoI*. The *rpoZ* insert was excised from
496 pUT18-rpoZ by digestion with *ScaI*, *HindIII*, and *XbaI*, and ligated into *HindIII*/*XbaI*-digested
497 pKNT25-*NcoI*.

498 *pUT18/KT25-gp4.2/gp1.5/gp8/gp6.5*

499 An *NcoI* restriction site was introduced into pUT18C (YZ709) by site-directed mutagenesis
500 using primers pYZ864 and pYZ866, generating pUT18C-*NcoI*. For pKT25 (YZ705), the
501 native *NcoI* site was first removed using primers pYZ863 and pYZ862, followed by
502 introduction of a new *NcoI* site using primers pYZ864 and pYZ865 to generate pKT25-*NcoI*.
503 Plasmids pET28-gp4.2, pET28-gp1.5, pET28-gp8, and pET28-gp6.5 were digested with
504 *EcoRI*, *NcoI*, and *HindIII*, and the resulting inserts were individually cloned into pUT18C-
505 *NcoI* or pKT25-*NcoI* vectors digested with *NcoI* and *HindIII*.

506 *Construction of Gp8 truncations*

507 Truncations of Gp8 were generated by site-directed mutagenesis of the *gp8* gene on the pKT25
508 vector in *E. coli* DH5α using the QuickChange method. Primer pairs pYZ1063/pYZ1064,
509 pYZ1065/pYZ1066, pYZ1067/pYZ1068, and pYZ1069/pYZ1070, were used to construct the
510 clip truncation, clip+stem truncation, N-terminal truncation, and C-terminal truncation,
511 respectively. PCR reactions were carried out with Q5 DNA polymerase using an extension
512 time of 3 min and an annealing temperature gradient of 50-70°C across eight 12 µL samples.
513 After amplification, the samples were pooled and digested with 2.5 µL *DpnI* at 37°C for 3 h,
514 followed by inactivation at 80°C for 20 min. The reaction mixture was then transformed into
515 *E. coli* DH5α via chemical transformation. Successful truncations were confirmed by Sanger
516 sequencing using primers pYZ471 and p472.
517

518 **Bacterial two-hybrid assay**

519 *E. coli* BTH101 was co-transformed with pUT18C and pKT25, where one plasmid carried
520 either *relA* or *spoT* and the other carried the phage gene of interest. Transformants were selected
521 on LB agar supplemented with 0.2% glucose, 25 µg/mL kanamycin and 100 µg/mL ampicillin
522 and incubated at 37°C. Overnight cultures were grown at 37°C with shaking at 170 rpm. The

523 following day, cells were washed twice in PBS, then resuspended in PBS to an OD_{600nm} of 5.
524 Subsequently, 5 µL normalized cell suspension was spotted onto LB agar with 0.2% glucose,
525 25 µg/mL kanamycin, 100 µg/mL ampicillin, and 40 µg/mL X-gal. Plates were incubated at
526 30°C overnight.
527
528 **Cloning of the pET28-HMS-relA and -spoT vectors**
529 *pET28-HMS-spoT* and derivatives
530 Plasmids pET28a and pMAL-c2x were digested with *NdeI* and *EcoRI* and ligated to generate
531 pET28-His_6-MBP (YZ913). The *sumo* and *spoT* genes were PCR-amplified using primers
532 pYZ692/693 and pYZ694/695, fused by overlap PCR, and cloned into pET28a using *NcoI* and
533 *HindIII* to generate pET28a-His_6-SUMO-SpoT (YZ307). The SUMO-SpoT fragment was
534 excised with *EcoRI* and *HindIII* and ligated into pET28a-His_6-MBP. Missing SUMO sequences
535 were amplified using primers pYZ684/685, digested with *EcoRI*, and inserted into this
536 intermediate construct to generate pET28-His_6-MBP-SUMO-SpoT (pET28-HMS-spoT).
537
538 *Generation of SpoT point mutants*
539 The E319Q and H72A/D73A mutations were introduced into pET28-HMS-spoT using PCR-
540 amplified fragments derived from chromosomal *spoT* mutant strains YZ586 and YZ905,
541 respectively[50]. PCR products generated with primers pYZ702 and pYZ703 were digested with
542 *PmlI* and *SalI* and ligated into pET28-HMS-spoT to generate the corresponding mutant
543 constructs. The *spoT* gene was deleted from pET28-HMS-spoT using primers pYZ905 and
544 pYZ906 to generate the pET28b-HMS vector (YZ1515).
545
546 Construction of *pET28-HMS-relA*

547 The *relA* gene was PCR-amplified from *E. coli* MG1655 using primers pYZ927 and pYZ928.
548 Both the PCR product and pET28b-HMS were digested with *BamHI* and *HindIII*, ligated using
549 T4 DNA ligase, and transformed into *E. coli* DH5α to generate pET28-HMS-relA.
550
551 **Co-immunoprecipitation**
552 Overnight cultures of *E. coli* BL21 DE3 strains expressing pRARE, pET28b-HMS, -*relA* or -
553 *spoT*, and pBAD30-*gp8-Flag* (see Strain list) were incubated in LB medium with 25 µg/mL
554 kanamycin, 25 µg/mL chloramphenicol, and 30 µg/mL ampicillin at 37°C with shaking at 160
555 rpm. The following day, cultures were back-diluted to an OD_{600nm} of 0.05 in 50 mL fresh LB
556 medium containing the same antibiotics as above and incubated at 37°C with shaking at 160
557 rpm until reaching OD_{600nm} of ~ 0.2-0.3. Gene expression was induced by addition of arabinose
558 and IPTG to final concentrations of 0.2% and 0.5 mM, respectively, followed by incubation
559 for 4 hours at 37°C with shaking at 160 rpm. Cells were harvested by centrifugation (10 min,
560 4000 rpm, 4°C), resuspended in 10 mL PBS and centrifuged again as above. Supernatant was
561 discarded and cell pellets were stored at -20°C. Pellets were thawed on ice, resuspended in 400
562 µL lysis buffer (50 mM HEPES (pH 8), 0.25 M NaCl, 10 mM imidazole, 200 µM $ZnCl_2$, and
563 2 mM $MgCl_2$) and disrupted with glass beads (Sigma, G4649) using a MagNA Lyser (20 s at
564 6500 rpm, done twice with cooling on ice between runs). Lysates were centrifuged (5 min,
565 5000 rpm, 4°C) and supernatants were collected. Total protein concentration was measured via
566 Bradford Assay, and samples were normalized with lysis buffer to equal total protein
567 concentrations. Equal volumes of normalized lysates were incubated with 50 µL Ni-NTA
568 Agarose resins (Qiagen) overnight at 4°C with gentle inversion. The next day, samples were
569 centrifuged (2 min, 1000 rpm, 4°C), and supernatant was removed. Resins were gently
570 resuspended with 1 mL lysis buffer and incubated for 1 h at 4°C with gentle inversion. Samples
571 were centrifuged (2 min, 1000 rpm, 4°C), and supernatant was removed. Resins were

572 subsequently resuspended in 1 mL wash buffer (50 mM HEPES (pH 8), 0.25 M NaCl, 20 mM
573 imidazole, 200 µM $ZnCl_2$, 2 mM $MgCl_2$) and incubated for 1 h at 4°C with gentle inversion.
574 Following incubation, samples were transferred to a 0.5 mL Eppendorf tube and centrifuged
575 (first for 2 min at 1000 rpm, then for 1 min at 13000 rpm). Supernatant was removed and
576 proteins were eluted with 20 µL elution buffer (50 mM HEPES (pH 8), 0.25 M NaCl, 1.25 M
577 imidazole, 200 µM $ZnCl_2$, 2 mM $MgCl_2$) to yield a final imidazole concentration of
578 approximately 500 mM). Samples were incubated for 15 min at 4°C (gently disturbing the
579 resins occasionally). Samples were then centrifuged (2 min, 1000 rpm), and 35 µL supernatant
580 was transferred to 11.6 µL 4x Leammli buffer, boiled for 15 min at 95°C and 12 µL of each
581 sample was loaded onto a 10% SDS-PAGE gel. Following electrophoresis, proteins were
582 transferred to a PVDF membrane by wet transfer (300 mA, 1 h, 4°C) using transfer buffer
583 composed of 20% methanol, 0.2 M glycine, and 25 mM Tris (pH 8.3). Membrane was blocked
584 overnight at 4°C in TBST + 5% (w/v) milk powder. Next day, the membrane was incubated
585 with anti-FLAG primary antibody diluted in TBST + 5% (w/v) milk powder for 1 h, 4°C,
586 washed three times (10 min each) in TBST, and subsequently incubated with anti-mouse
587 secondary antibody in TBST + 5% (w/v) milk powder for 1 h, 4°C. After three additional
588 washes in TBST, the membrane was developed using Pierce® ECL Western Blotting Substrate
589 (Thermo Scientific, #32209) for 1 min and imaged via ImageQuant LAS4000.
590

591 **Protein purification for biochemical assays**

592 RelA (YZ1607), SpoT hydrolysis only (HYD, YZ1063), SpoT synthesis only (SYN, YZ1070),
593 and Gp8 (YZ1632) constructs bearing an N-terminal His–MBP–SUMO (HMS) tag were
594 expressed from pET28b in *E. coli* BL21(DE3). Overnight cultures of these strains were grown
595 in LB medium supplemented with appropriate antibiotics at 37°C, with shaking at 160 rpm.
596 The following day, cultures were back-diluted 1:50 into 0.5-1 L fresh LB medium

597 supplemented with appropriate antibiotics and grown at 37°C with shaking at 160 rpm until
598 reaching an OD of 0.4-0.7. Protein expression was induced by the addition of IPTG to a final
599 concentration of 0.1 mM, and cultures were incubated overnight at 24°C, shaking with aeration.
600 The next day, cells were harvested by centrifugation (5000 rpm, 10 min, 4°C), washed in 30
601 mL cold PBS, and pelleted again (4000 rpm, 20 min, 4°C). Resulting pellets were resuspended
602 in 40 mL cold lysis buffer (50 mM Tris-HCl pH=8, 1 M NaCl, 2 mM DTT, 10 mM imidazole)
603 supplemented with Pierce™ Protease Inhibitor Mini (Thermo Scientific, A32955). Cells were
604 lysed by sonication on ice for 24 min at 20% amplitude, and lysates were cleared by
605 centrifugation (14000 rpm for 45 min at 4 °C). Cleared lysates were incubated with 0.5-1 mL
606 Ni-NTA Agarose resins (Qiagen) overnight at 4°C with gentle inversion. The next day, the
607 resins were collected by centrifugation (1000 rpm, 2 min) and washed once with 30 mL lysis
608 buffer (1 h, 4°C), followed by 30 mL wash buffer (same composition as lysis buffer, except
609 imidazole increased to 20 mM). Resins were transferred onto a Bio-Rad Gravity Flow Column,
610 and bound proteins were eluted with 700 µL elution buffer (50 mM tris-HCl pH=8, 1 M NaCl,
611 2 mM DTT, 500 mM imidazole). The eluted fraction was subjected to size-exclusion
612 chromatography using an ÄKTA Pure™ system (Cytiva) equilibrated gel filtration buffer (50
613 mM HEPES pH=8, 1 M NaCl, 2 mM DTT, 5% glycerol). Protein concentrations were
614 determined via Bradford Assay.
615
616 **Synthesis of [α-^{32}P](p)ppGpp via RelSeq**
617 [α-^{32}P](p)ppGpp was synthesized using[α-^{32}P]GTP (revvity, BLU006X250UC) as substrate in
618 a RelSeq-catalyzed reaction[48]. RelSeq (YZ8) was expressed and purified as described above
619 except that protein expression was induced with 0.5 mM IPTG for 3 h at 30°C. The purification
620 buffer contained 500 mM NaCl, 50 mM Tris-HCl (pH 8), and 5% glycerol, with imidazole
621 concentrations of 20, 40, and 500 mM for lysis, wash, and elution buffers, respectively. The

622 gel filtration buffer was identical but without imidazole. For the enzyme reaction, a 10×
623 reaction buffer was prepared containing 250 mM Tris (pH 9), 1 M NaCl, and 150 mM $MgCl_2$.
624 The final reaction system contained 1× reaction buffer, 8 mM ATP, 125 nM [α-^{32}P]GTP, and
625 4 μM RelSeq, and was incubated at 37°C for 1 h. The reaction was terminated by boiling for 5
626 min at 95°C, followed by centrifugation (14000 rpm, 5 min). Conversion of substrate was
627 verified by thin-layer chromatography (TLC) using 0.5 μL of the reaction mixture and 1.5 M
628 KH_2PO_4 (pH 3.4) as the mobile phase.
629
630 **Biochemical assays**
631 Synthetase activity of RelA and SpoT (SYN), was assayed in reaction mixtures containing 50
632 mM HEPES (pH 7.4), 100 mM KCl, 5 mM $MgCl_2$, 2 mM DTT, 0.2 mg/mL BSA, 2 mM GTP,
633 and 6 nM [α-^{32}P]GTP (revvity, BLU006X250UC) were prepared. Protein was added to final
634 concentrations of 0.5 μM (RelA) or 3 μM (SpoT (SYN)). Gp8 was added to varying final
635 concentrations, and samples were incubated at room temperature for 10 min before enzyme
636 reactions were initiated by addition of 5 mM ATP. Hydrolase activity of SpoT (HYD) was
637 assayed in a reaction mixture containing 50 mM HEPES (pH 8), 100 mM KCl, 5 mM $MnCl_2$,
638 2 mM DTT, and 0.2mg/mL BSA was prepared. SpoT (HYD) was added to a final concentration
639 of 100 nM, while Gp8 was added at varying final concentrations. Reaction mixtures were
640 incubated at room temperature for 10 min before enzyme reaction was initiated by the
641 simultaneous addition of ppGpp (Jena Biocience, NU-884L), and hot [α-^{32}P](p)ppGpp to final
642 concentrations of 31.25 and 6 nM, respectively. Enzyme reactions were stopped by transferring
643 4 μL of the reaction mixtures into 1 μL cold 250 mM EDTA (final concentration 50 mM).
644 Samples were loaded onto a PEI Cellulose plates and resolved using 1.5 M KH_2PO_4 (pH 3.4)
645 as the mobile phase. Plates were exposed to a BAS-MS imaging plate and scanned using a
646 Typhoon phosphorimager.

647

648 **Phage handling and propagation**

649 Phages were propagated using *E. coli* MG1655 as host. A 50 mL MG1655 culture in LB
650 supplemented with 1 mM $MgCl_2$ and 1 mM $CaCl_2$ was grown at 37°C with shaking at 160 rpm
651 to an OD_{600nm} of ~ 0.5. Phage stock (100 µL; PFU ~10^8-10^{10}) was added and incubation was
652 continued until extensive lysis was observed (1-3 h for T7). The lysate was treated with
653 chloroform (1 mL per 10 mL culture), vortexed, incubated for 5-10 min at room temperature,
654 and centrifuged (5 min, 5000 rpm). The supernatant was transferred to a new tube, centrifuged
655 again and collected into a clean tube. The phage stock was concentrated, and the buffer was
656 exchanged following the protocol described here[51]. Briefly, a 5× PEG solution (5 M NaCl, 20%
657 (w/v) PEG800) was added to the cleared lysate and incubated overnight at 4°C. The
658 precipitated phages were pelleted (1 h, 4°C, 19000 g), resuspended in 0.5-1 mL phage buffer
659 (150 mM NaCl, 40 mM Tris, 10 mM $MgSO_4$), and PFU was determined via plaque assay.
660 Phage stocks were stored at 4°C.

661

662 **Plaque assay**

663 Plaque assays were performed as described here[52]. Briefly, cultures of the appropriate strains
664 were prepared in LB with appropriate antibiotics and incubated overnight at 37°C shaking at
665 160 rpm. The following day, cultures were adjusted to OD_{600nm}=2, and 200 µL normalized
666 culture was mixed with 100 µL of 10-fold serially diluted phage and incubated at room
667 temperature for 10 min. The mixtures were then mixed with 3 ml melted 0.7% LB agar (kept
668 at 50°C) and immediately poured onto prewarmed 1% LB agar plates. Plates were incubated
669 overnight at 37°C.

670

671 **Liquid killing assay**

672 *E. coli* strains MG1655, Δ*relA*, and Δ*relA*Δ*spoT*, were incubated overnight in LB medium at
673 37°C with shaking at 160 rpm. The following day, cultures were backdiluted into fresh LB
674 medium and incubated in flasks at 37°C with shaking at 160 rpm until reaching an OD_{600nm} of
675 ~ 0.4. Cultures were normalized to OD_{600nm}=0.4, and 150 µL normalized culture was mixed
676 with T7 phage in a clear 96-well plate to the desired MOIs. The OD_{600nm} was recorded every
677 five minutes at 37°C without shaking.
678
679 **T7 phage engineering**
680 To enable targeted mutagenesis of the essential T7 *gp8* gene, we established a genetic
681 dependency between the host and the phage based on the *trxA* gene, which is a host factor
682 essential for T7 replication. The endogenous *trxA* gene was deleted from the host chromosome,
683 rendering the host non-permissive to wild-type T7 infection. To restore infectivity, *trxA* was
684 introduced into the T7 genome via homologous recombination in place of *gp8*, and the *gp8* was
685 instead provided on the plasmid vector pCA24N[53] transformed to this Δ*trxA* host. This created
686 an interdependent system where the *gp8* sequence on the plasmid could be easily manipulated
687 prior to transformation. Due to homology sequences, the plasmid-encoded *gp8* mutant could
688 integrate into its original position on the T7 genome and thus create a mutant T7 particle that
689 can be counter selected using its independence of a plasmid borne *gp8*.
690
691 **Delete *trxA* in MG1655 using P1 phage transduction**
692 To delete *trxA* from *E. coli* MG1655, a P1 lysate was first prepared using *E. coli* Δ*trxA* strain
693 from the Keio collection[54]. Then, the P1 transduction method was used to generate a MG1655
694 Δ*trxA::kan* strain[55] and the kanamycin resistance maker was flipped out by using pCP20[56].
695
696 **Replace *gp8* with *trxA* in T7**

697 The *trxA* gene was PCR-amplified using genomic DNA from *E. coli* strain MG1655 as a
698 template and primers pYZ1189 and pYZ1190, each containing 40 bp extensions homologous
699 to sequences flanking the *gp8* locus in the T7 phage genome. The purified PCR product was
700 introduced into *E. coli* MG1655 cells by electroporation during co-infection with T7 phage.
701 Immediately following electroporation, LB medium was added, and the culture was incubated
702 at 37°C,160 rpm until lysis was observed (around 1.5 hours). Phage lysates were then harvested
703 with chloroform and clarified via centrifugation (5 min, 5000 rpm).
704
705 **Cloning of pCA24N-gp8 and quick-change mutagenesis of *gp8***
706 The *gp8* gene as well as 350 bp flanking regions from T7 was PCR amplified using primers
707 pYZ1191 and pYZ1192 that also encoded a *XhoI* and *HindIII* restriction site, respectively. This
708 PCR product as well as the pCA24N[53] plasmid were both digested with *XhoI* and *HindIII* and
709 ligated together using T4 ligase. The constructed pCA24N-gp8 was purified and used as
710 template for quick-change mutagenesis with primers pYZ1085-pYZ1136 (see Primer list).
711
712 **Constructing mutant T7 phages with *gp8* mutations**
713 pCA24N plasmids encoding mutant *gp8* were purified and transformed into *E. coli* MG1655
714 Δ*trxA*. This strain was then infected with T7 *gp8::trxA* phage lysate (prepared as described
715 above). Through homologous recombination between the plasmid-encoded *gp8* mutant and
716 the corresponding flanking regions in the T7 genome (where *trxA* is inserted), the mutant *gp8*
717 sequence can replace *trxA*, and results in T7 progeny that carry the desired *gp8* mutation. The
718 mutant T7 phage particles can be counter selected using its independence of the pCA24N-
719 gp8.
720
721 **Measurement of (p)ppGpp by radiolabeling and autoradiography**

722 (p)ppGpp is a very labile molecule not suited for analysis by HPLC or mass spectrometry[57].
723 We therefore, performed thin layer chromatography (TLC) to quantify both pppGpp and ppGpp.
724 As phosphates in the medium impairs efficient incorporation of $H_3{}^{32}PO_4$ during labelling,
725 MOPS medium supplemented with 0.2 mM K_2HPO_4 (low phosphate concentration), and 0.2%
726 (v/v) glucose was used[41]. MG1655 was grown for ca. 18 hrs in MOPS-lowP_i-Glc media at
727 37 °C with agitation (160 rpm). Afterwards, the strains were adjusted to OD_{600nm}=0.05 in
728 MOPS-lowP_i-Glc and grown at 37 °C with agitation (160 rpm) until OD_{600nm} of 0.2-0-3 was
729 reached. Then, cells were transferred to a 2-ml Eppendorf tube and $H_3{}^{32}PO_4$ was added, equal
730 to 100 µCi/ml (Revvity, NEX053001MC). After 1.5 h at 37 °C with 600 rpm agitation, cells
731 were transferred to a new tube and infected with phage to an MOI of 0.1. Immediately after,
732 150 µl infected cells were transferred to a clear 96-well plate and OD_{600nm} at 37°C was
733 monitored every 2 min via a plate reader (BioTek). Simultaneously, 25 µl sample was collected
734 every 2 min and transferred to 5 µl cold 2 M formic acid. Samples were stores at -20°C until
735 analysed by TLC using 1.5 M KH_2PO_4 (pH 3.4) as mobile phase.

Acknowledgements

We would like to thank Jeppe Aaby Andersen for cloning of the portal protein from phages P1 and N4 into the bacterial two-hybrid system, and for testing their interaction with RelA and SpoT. We would also like to thank Sonia de Araujo and Anette Vestergaard for cloning of the *relA*, *spoT* and their truncates into the bacterial two-hybrid system. We thank Yueyue Liu for preparing stocks of the selected phages obtained from the BASEL Collection. We are grateful for Michael J Gray's gifting of the RNAP SR strains. The work is supported by a Danmarks Frie Forskningsfond grant (2032-00030B) and the Carlsberg Foundation Semper Ardens Accelerate grant (CF24-1843) to Y.E.Z. and the Chinese Scholarship Council program (202006330098) to L.K.W.

References

1 Potrykus, K. & Cashel, M. (p)ppGpp: still magical? *Annual review of microbiology* **62**, 35-51 (2008). https://doi.org/10.1146/annurev.micro.62.081307.162903

2 Anderson, B. W., Fung, D. K. & Wang, J. D. Regulatory Themes and Variations by the Stress-Signaling Nucleotide Alarmones (p)ppGpp in Bacteria. *Annu Rev Genet* **55**, 115-133 (2021). https://doi.org/10.1146/annurev-genet-021821-025827

3 Irving, S. E., Choudhury, N. R. & Corrigan, R. M. The stringent response and physiological roles of (pp)pGpp in bacteria. *Nat Rev Microbiol* **19**, 256-271 (2021). https://doi.org/10.1038/s41579-020-00470-y

4 Hauryliuk, V., Atkinson, G. C., Murakami, K. S., Tenson, T. & Gerdes, K. Recent functional insights into the role of (p)ppGpp in bacterial physiology. *Nat Rev Microbiol* **13**, 298-309 (2015). https://doi.org/10.1038/nrmicro3448

5 Hobbs, J. K. & Boraston, A. B. (p)ppGpp and the Stringent Response: An Emerging Threat to Antibiotic Therapy. *ACS Infectious Diseases* **5**, 1505-1517 (2019). https://doi.org/10.1021/acsinfecdis.9b00204

6 Das, B. & Bhadra, R. K. (p)ppGpp Metabolism and Antimicrobial Resistance in Bacterial Pathogens. *Front Microbiol* **11**, 563944 (2020). https://doi.org/10.3389/fmicb.2020.563944

7 Harms, A., Maisonneuve, E. & Gerdes, K. Mechanisms of bacterial persistence during stress and antibiotic exposure. *Science* **354** (2016). https://doi.org/10.1126/science.aaf4268

8 Dalebroux, Z. D., Svensson, S. L., Gaynor, E. C. & Swanson, M. S. ppGpp conjures bacterial virulence. *Microbiology and molecular biology reviews : MMBR* **74**, 171-199 (2010). https://doi.org/10.1128/MMBR.00046-09

9 Tabib-Salazar, A. *et al.* T7 phage factor required for managing RpoS in Escherichia coli. *Proc Natl Acad Sci U S A* **115**, E5353-E5362 (2018). https://doi.org/10.1073/pnas.1800429115

10 Nowicki, D., Kobiela, W., Wegrzyn, A., Wegrzyn, G. & Szalewska-Palasz, A. ppGpp-dependent negative control of DNA replication of Shiga toxin-converting bacteriophages in Escherichia coli. *J Bacteriol* **195**, 5007-5015 (2013). https://doi.org/10.1128/JB.00592-13

11 Dedrick, R. M. *et al.* Prophage-mediated defence against viral attack and viral counter-defence. *Nat Microbiol* **2**, 16251 (2017). https://doi.org/10.1038/nmicrobiol.2016.251

12 Zhang, Y. E. Protein Kinases in Mediating Phage-Bacteria Interactions. *Kinases and Phosphatases* **3**, 14 (2025).

13 Egido, J. E., Costa, A. R., Aparicio-Maldonado, C., Haas, P. J. & Brouns, S. J. J. Mechanisms and clinical importance of bacteriophage resistance. *FEMS Microbiol Rev* **46** (2022). https://doi.org/10.1093/femsre/fuab048

14 Haseltine, W. A. & Block, R. Synthesis of guanosine tetra- and pentaphosphate requires the presence of a codon-specific, uncharged transfer ribonucleic acid in the acceptor site of ribosomes. *Proc Natl Acad Sci U S A* **70**, 1564-1568 (1973). https://doi.org/10.1073/pnas.70.5.1564

15 Xiao, H. *et al.* Residual guanosine 3',5'-bispyrophosphate synthetic activity of relA null mutants can be eliminated by spoT null mutations. *J Biol Chem* **266**, 5980-5990 (1991).

16 Fernández-Coll, L. & Cashel, M. Possible Roles for Basal Levels of (p)ppGpp: Growth Efficiency Vs. Surviving Stress. *Front Microbiol* **11**, 592718 (2020). https://doi.org/10.3389/fmicb.2020.592718

17 Seyfzadeh, M., Keener, J. & Nomura, M. spoT-dependent accumulation of guanosine tetraphosphate in response to fatty acid starvation in Escherichia coli. *Proc Natl Acad Sci U S A* **90**, 11004-11008 (1993).

18 Vinella, D., Albrecht, C., Cashel, M. & D'Ari, R. Iron limitation induces SpoT-dependent accumulation of ppGpp in Escherichia coli. *Mol Microbiol* **56**, 958-970 (2005). https://doi.org/10.1111/j.1365-2958.2005.04601.x

19 Spira, B., Silberstein, N. & Yagil, E. Guanosine 3',5'-bispyrophosphate (ppGpp) synthesis in cells of Escherichia coli starved for Pi. *J Bacteriol* **177**, 4053-4058 (1995). https://doi.org/10.1128/jb.177.14.4053-4058.1995

20 Ross, W., Vrentas, C. E., Sanchez-Vazquez, P., Gaal, T. & Gourse, R. L. The magic spot: a ppGpp binding site on E. coli RNA polymerase responsible for regulation of transcription initiation. *Mol Cell* **50**, 420-429 (2013). https://doi.org/10.1016/j.molcel.2013.03.021

21 Ross, W. *et al.* ppGpp Binding to a Site at the RNAP-DksA Interface Accounts for Its Dramatic Effects on Transcription Initiation during the Stringent Response. *Mol Cell* **62**, 811-823 (2016). https://doi.org/10.1016/j.molcel.2016.04.029

22 Sanchez-Vazquez, P., Dewey, C. N., Kitten, N., Ross, W. & Gourse, R. L. Genome-wide effects on Escherichia coli transcription from ppGpp binding to its two sites on RNA polymerase. *Proceedings of the National Academy of Sciences* **116**, 8310-8319 (2019). https://doi.org/doi:10.1073/pnas.1819682116

23 Lewis, K. Persister cells, dormancy and infectious disease. *Nature Reviews Microbiology* **5**, 48-56 (2007). https://doi.org/10.1038/nrmicro1557

24 Schrader, H. S. *et al.* Bacteriophage infection and multiplication occur in Pseudomonas aeruginosa starved for 5 years. *Can J Microbiol* **43**, 1157-1163 (1997). https://doi.org/10.1139/m97-164

25 Bryan, D., El-Shibiny, A., Hobbs, Z., Porter, J. & Kutter, E. M. Bacteriophage T4 Infection of Stationary Phase E. coli: Life after Log from a Phage Perspective. *Front Microbiol* **7**, 1391 (2016). https://doi.org/10.3389/fmicb.2016.01391

26 Ho, P. *et al.* Bacteriophage antidefense genes that neutralize TIR and STING immune responses. *Cell Rep* **42**, 112305 (2023). https://doi.org/10.1016/j.celrep.2023.112305

27 Bae, B. *et al.* Phage T7 Gp2 inhibition of Escherichia coli RNA polymerase involves misappropriation of sigma70 domain 1.1. *Proceedings of the National Academy of Sciences* **110**, 19772-19777 (2013). https://doi.org/doi:10.1073/pnas.1314576110

28 Gray Michael, J. Inorganic Polyphosphate Accumulation in Escherichia coli Is Regulated by DksA but Not by (p)ppGpp. *Journal of Bacteriology* **201**, 10.1128/jb.00664-00618 (2019). https://doi.org/10.1128/jb.00664-18

29 Gray Michael, J. Interactions between DksA and Stress-Responsive Alternative Sigma Factors Control Inorganic Polyphosphate Accumulation in Escherichia coli. *Journal of Bacteriology* **202**, 10.1128/jb.00133-00120 (2020). https://doi.org/10.1128/jb.00133-20

30 Cuervo, A. *et al.* Structural characterization of the bacteriophage T7 tail machinery. *J Biol Chem* **288**, 26290-26299 (2013). https://doi.org/10.1074/jbc.M113.491209

31 Jensen, J. D., Parks, A. R., Adhya, S., Rattray, A. J. & Court, D. L. λ Recombineering Used to Engineer the Genome of Phage T7. *Antibiotics (Basel)* **9** (2020). https://doi.org/10.3390/antibiotics9110805

32 Sarubbi, E., Rudd, K. E. & Cashel, M. Basal ppGpp level adjustment shown by new spoT mutants affect steady state growth rates and rrnA ribosomal promoter regulation in Escherichia coli. *Molecular and General Genetics MGG* **213**, 214-222 (1988). https://doi.org/10.1007/BF00339584

33 Maffei, E. *et al.* Systematic exploration of Escherichia coli phage-host interactions with the BASEL phage collection. *PLoS Biol* **19**, e3001424 (2021). https://doi.org/10.1371/journal.pbio.3001424

34 Qimron, U., Kulczyk, A. W., Hamdan, S. M., Tabor, S. & Richardson, C. C. Inadequate inhibition of host RNA polymerase restricts T7 bacteriophage growth on hosts overexpressing udk. *Mol Microbiol* **67**, 448-457 (2008). https://doi.org/10.1111/j.1365-2958.2007.06058.x

35 Kingston, R. E., Nierman, W. C. & Chamberlin, M. J. A direct effect of guanosine tetraphosphate on pausing of Escherichia coli RNA polymerase during RNA chain elongation. *Journal of Biological Chemistry* **256**, 2787-2797 (1981). https://doi.org/https://doi.org/10.1016/S0021-9258(19)69683-3

36 Tabib-Salazar, A. & Wigneshweraraj, S. RNA Management During T7 Infection. *Phage (New Rochelle)* **3**, 136-140 (2022). https://doi.org/10.1089/phage.2022.0029

37 Savalia, D., Robins, W., Nechaev, S., Molineux, I. & Severinov, K. The role of the T7 Gp2 inhibitor of host RNA polymerase in phage development. *J Mol Biol* **402**, 118-126 (2010). https://doi.org/10.1016/j.jmb.2010.07.012

38 Severinova, E. & Severinov, K. Localization of the Escherichia coli RNA polymerase beta' subunit residue phosphorylated by bacteriophage T7 kinase Gp0.7. *J Bacteriol* **188**, 3470-3476 (2006). https://doi.org/10.1128/jb.188.10.3470-3476.2006

39 Rodnina, M. V. Translation in Prokaryotes. *Cold Spring Harb Perspect Biol* **10** (2018). https://doi.org/10.1101/cshperspect.a032664

40 Casjens, S. R. The DNA-packaging nanomotor of tailed bacteriophages. *Nat Rev Microbiol* **9**, 647-657 (2011). https://doi.org/10.1038/nrmicro2632

41 Zhang, Y. E. *et al.* (p)ppGpp Regulates a Bacterial Nucleosidase by an Allosteric Two-Domain Switch. *Mol Cell* **74**, 1239-1249.e1234 (2019). https://doi.org/10.1016/j.molcel.2019.03.035

42 Grucela, P. K., Fuhrer, T., Sauer, U., Chao, Y. & Zhang, Y. E. Ribose 5-phosphate: the key metabolite bridging the metabolisms of nucleotides and amino acids during stringent response in Escherichia coli? *Microb Cell* **10**, 141-144 (2023). https://doi.org/10.15698/mic2023.07.799

43 Wang, B. *et al.* Affinity-based capture and identification of protein effectors of the growth regulator ppGpp. *Nat Chem Biol* **15**, 141-150 (2019). https://doi.org/10.1038/s41589-018-0183-4

44 Wang, B., Grant, R. A. & Laub, M. T. ppGpp Coordinates Nucleotide and Amino-Acid Synthesis in E. coli During Starvation. *Mol Cell* **80**, 29-42.e10 (2020). https://doi.org/10.1016/j.molcel.2020.08.005

45 Stano, N. M. & Patel, S. S. T7 lysozyme represses T7 RNA polymerase transcription by destabilizing the open complex during initiation. *J Biol Chem* **279**, 16136-16143 (2004). https://doi.org/10.1074/jbc.M400139200

46 Zhang, X. & Studier, F. W. Multiple Roles of T7 RNA Polymerase and T7 Lysozyme During Bacteriophage T7 Infection. *Journal of Molecular Biology* **340**, 707-730 (2004). https://doi.org/https://doi.org/10.1016/j.jmb.2004.05.006

47 Nozaki, S. & Niki, H. Exonuclease III (XthA) Enforces In Vivo DNA Cloning of Escherichia coli To Create Cohesive Ends. *J Bacteriol* **201** (2019). https://doi.org/10.1128/jb.00660-18

48 Zhang, Y., Zborníková, E., Rejman, D. & Gerdes, K. Novel (p)ppGpp Binding and Metabolizing Proteins of Escherichia coli. *mBio* **9** (2018). https://doi.org/10.1128/mBio.02188-17

49 Schicketanz, M. L., Dlugosz, P. & Zhang, Y. E. Identifying the Binding Proteins of Small Ligands with the Differential Radial Capillary Action of Ligand Assay (DRaCALA). *J Vis Exp* (2021). https://doi.org/10.3791/62331

50 Liu, Y. *et al.* Basal ppGpp regulation by SpoT coordinates metabolic homeostasis and acid resistance. *bioRxiv*, 2026.2001.2026.700336 (2026). https://doi.org/10.64898/2026.01.26.700336

51 Borges, A. & Athukoralage, J. *Phage amplification and concentration*, <https://www.protocols.io/view/phage-amplification-and-concentration-yxmvmnb86g3p/v1/references> (2022).

52 Ceelen, M. *Plaque assay*, <https://www.protocols.io/view/plaque-assay-kqdg35ebqv25/v1> (2019).

53 Kitagawa, M. *et al.* Complete set of ORF clones of Escherichia coli ASKA library (A Complete Set of E. coli K-12 ORF Archive): Unique Resources for Biological Research. *DNA Research* **12**, 291-299 (2006). https://doi.org/10.1093/dnares/dsi012

54 Baba, T. *et al.* Construction of Escherichia coli K-12 in-frame, single-gene knockout mutants: the Keio collection. *Mol Syst Biol* **2**, 2006.0008 (2006). https://doi.org/10.1038/msb4100050

55 Thomason, L. C., Costantino, N. & Court, D. L. E. coli genome manipulation by P1 transduction. *Curr Protoc Mol Biol* **Chapter 1**, 1 17 11-11 17 18 (2007). https://doi.org/10.1002/0471142727.mb0117s79

56 Cherepanov, P. P. & Wackernagel, W. Gene disruption in Escherichia coli: TcR and KmR cassettes with the option of Flp-catalyzed excision of the antibiotic-resistance determinant. *Gene* **158**, 9-14 (1995). https://doi.org/10.1016/0378-1119(95)00193-a

57 Varik, V., Oliveira, S. R. A., Hauryliuk, V. & Tenson, T. HPLC-based quantification of bacterial housekeeping nucleotides and alarmone messengers ppGpp and pppGpp. *Sci Rep* **7**, 11022 (2017). https://doi.org/10.1038/s41598-017-10988-6